Observing Galaxies in Environments

Presented by Emma Lovett

University of Massachusetts Amherst

Commonwealth Honors College Thesis

Committee Chair: John Silverman, University of Tokyo

Committee Chair: Mauro Giavalisco, University of Massachusetts, Amherst

May, 2021

Abstract

This study addresses the origin of the observed bimodality in galaxy morphology that exists as early-type galaxies and late-type galaxies. Data is taken from the Hyper-Suprime Cam Subaru Strategic Program (HSC-SSP) to compare populations of galaxies at low redshifts of $0.01 < z < 0.20$ in different dark matter halo mass environments. Physical properties of galaxies such as radius, a light profile modeled with the Sérsic function, and the star formation rate are observed in three different environments: the field region (halo mass $<10^{13}$ solar mass), groups of galaxies (halo mass between 10^{13} and 10^{14} solar mass), and galaxy clusters (halo mass $>10^{14}$ solar mass). The results confirm that galaxies in groups and clusters are characterized by a Sérsic index in the range 2-8, which is typical of early-type, spheroidal galaxies. Galaxies in field regions, on the other hand, are often found to have Sérsic index in the range 0.3-2, which is typical of late-type, disk galaxies. A discussion of potential mechanisms that cause the observed environmental dependence of galaxy morphology is then included, with the most probable explanations being galaxy-galaxy mergers that affect the star-formation rates in the centers of galaxies, or otherwise randomize stellar orbits to change late-type disks into early-type ellipticals. Strangulation and ram-pressure stripping are also discussed, as there appear to be some discrepancies between Sérsic index and star formation rate based on previous studies. Strangulation is concluded as the most probable mechanism at play in the observed set of galaxies because there is a noticeable increase in stellar mass in quiescent galaxies. This study will hopefully provide additional insight into galaxy evolution addressing the fundamental dependence of morphology on environment.

Table of Contents

Chapter 1

Introduction

1.1 Background

1.1.1 Observed Bimodality in Galaxy Morphology

The inquiry of nature vs. nurture extends past the behavior of humanity, and applies to galaxy formation and evolution. Extragalactic astronomers have debated whether galaxies are formed solely based on the formation history of the dark matter haloes in which they reside (nature), or whether they evolve through various processes based on their environments (nurture). Several studies on the properties of galaxies and their morphologies have been conducted in the past, and have found evidence that points to environmental dependence of characteristics such as shape, color, and star formation rate (SFR). SFR is defined as the total

mass of stars formed in a galaxy per year, measured in solar masses. The three major environments that galaxies form in are based on dark matter halo mass, which changes as density increases, and are known as galaxy clusters, groups of galaxies, and field regions.

Galaxy clusters are the largest gravitationally-bound structures in the universe (Voit 2005). Groups of galaxies follow in the hierarchy of cosmological structures, and are equally as important in the study of galaxy evolution. The least dense environment galaxies form in is known as the field region. Within these three density regions, galaxies can be divided into two categories: early-type galaxies and late-type galaxies.

Early-type galaxies, in general, are red in color with low SFR and an elliptical shape. Late-type galaxies, on the other hand, are blue star-forming galaxies that take on a disk shape (Naab, Khochfar, & Burkert 2006). This division in classification is known as the bimodality of galaxy morphology in the universe, and is taken from the Hubble classification of galaxies. In both classifications of galaxies, both stellar dynamics and gas particle collisions play a large role in governing the shapes and SFR's. In late-type galaxies, it is theorized that gas settles into a disk in order to conserve angular momentum. This leads to little random motion in the orbits of stars within galaxies; instead, stars conform to circular orbits along the plane of the disks. A disk's thickness is determined by the balance between gravity and velocity dispersion, where velocity dispersion is measured through spectroscopy. Velocity dispersion measures the spread of vertical velocities of stars, and is often given by Equation 1:

$$\sigma_z^{\,2} = \overline{(v_z^{\,2} - \overline{(v_z)}^2)} \qquad (1)$$

where v_z is the vertical velocity and the bar over expression denotes the expected value over all stars. The velocity dispersion can be used alongside the Virial Theorem to derive a galaxy's stellar mass. It has been observed that stars in luminous elliptical galaxies following random motion have higher velocity dispersions than those of late-type galaxies (Sparke & Gallagher 2007).

On average, disk galaxies rotate at a faster rate than elliptical galaxies with higher kinetic energy, except for the galactic bulge, which may be comparable to an early-type galaxy despite its placement within a late-type disk. In early-type galaxies, SFR is generally much lower, and stellar orbits are more randomized than in the disk regions. This may be due to the fact that early-type galaxies are generally more massive than late-type galaxies (Vulcani, Poggianti, Aragón-Salamanca et al. 2011). Although elliptical galaxies may appear to have reached some state of equilibrium, these galaxies vary in rotational speeds and can either be classified as oblate elliptical galaxies or triaxial elliptical galaxies. For more on the stellar and gaseous dynamics within both early- and late-type galaxies, see e.g. Sparke & Gallagher, 2007.

Numerous studies have shown that the morphology-density relation observed in galaxy clusters (Dressler 1980) is also prevalent in galaxy groups (e.g. Postman & Geller 1984): at higher densities (i.e. in galaxy clusters), early-type galaxies occur more frequently, whereas late-type galaxies tend to prefer low-density environments (i.e. field regions). This fact has been verified by several following studies (e.g. Weinmann, Yang, Bosch, et al. 2006). Furthermore, because morphology and color are tightly correlated, a color-stellar mass relation has been observed at all local densities (Grützbauch, Conselice, Varela et al. 2011). A color-stellar mass relationship solidifies a color-density relation because it minimizes the possibility of external

factors affecting the environment to create invalid trends. Although there is a clear relationship between a galaxy's characteristics (i.e. SFR, stellar mass) and its halo mass, both Weinmann et al. (2006) and Tanaka et al. (2004) found a weaker correlation between galaxy characteristics and luminosity.

Weinmann et al. (2006) investigated the correlation between galaxy characteristics and halo mass, and found that the fraction of late-type galaxies decreases with increasing halo mass at a fixed luminosity. This correlation can be seen in Figure 1.1 (Figure 5 in Weinmann et al. (2006)). Figure 1.1 shows the fraction of late-type (left), early-type (center), and intermediate-type (right) galaxies against increasing halo mass. The trend is consistent for all early- and late-type galaxies, despite their positions as central (middle row) or satellite (bottom row) galaxies in the group.

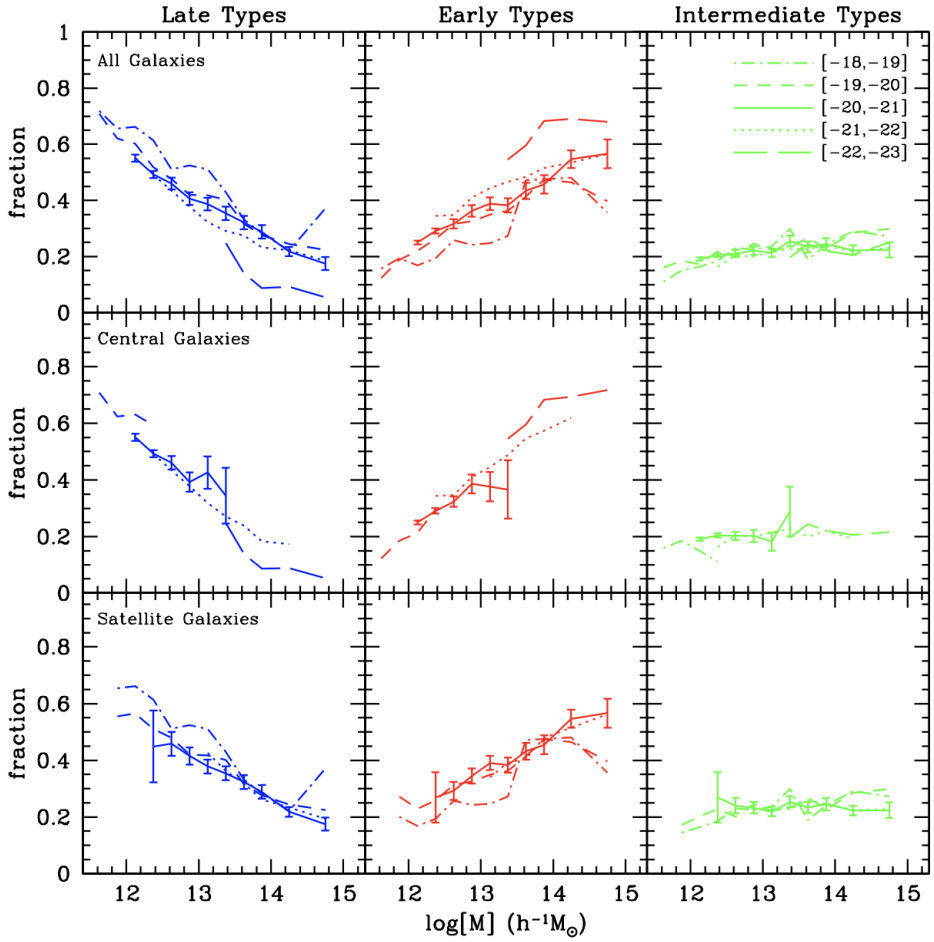

Figure 1.1. (Figure 5 from Weinmann et al. (2006) that shows the fraction of early-, late-, and intermediate-type galaxies in different regions of the dark matter halo mass.

It has also been found in the same light that these early-type galaxies in denser regions have a suppressed SFR compared to the late-type galaxies that exist in the field, which may be explained by strangulation (Tanaka, Goto, Okamura, et al. 2004). Strangulation and other theorized mechanisms of environmental dependence will be further discussed in section 1.2.

The distinction between early-type galaxies and late-type galaxies is the root of many questions in galaxy morphology, and the origin of this observed bimodality is addressed in several studies. Mandelbaum, Seljak, Kauffmann et al. (2006) used galaxy-galaxy lensing to observe the fraction of early- and late-type galaxies as the amount of dark matter varied in environments. Aside from galaxy-galaxy lensing, there are several opposing methods used for galaxy observation, such as X-Ray emissions to observe poor-groups and the intra-group gas within (Zabludoff & Mulchaey, 1998) and emissions in the optical band, which is what the Hyper-Suprime Cam Subaru Strategic Program (HSC-SSP) can be used for (Aihara, AlSayyad, Ando et al. 2019). In addition to various observational methods, there exist several quantities to relate to galaxy morphology, such as luminosity function (Tempel, Saar, Liivamägi et al. 2011) and halo mass, as discussed previously. Despite the numerous studies that have been done to illustrate the relationship between environment and galaxy characteristics, little research has been done on galaxies at low redshifts in the Yang et al. (2005) group catalog using the HSC-SSP, despite it being the most powerful optical imaging survey of the decade (Miyazaki & Iwata 2014).

1.2 Theorized Mechanisms Behind Environmental Dependence

There are several processes that have been studied to explain the observed correlation between galaxy morphology and environment. The amount of hot gas available in an environment is found in several studies to affect the galaxies that exist within the region, as gas temperature is linked specifically to star formation rate (SFR) (e.g. Kawata & Mulchaey 2008).

Stellar orbits and gas dynamics within galaxies, as previously mentioned, also play a role in morphology. This report will focus on three theorized mechanisms that may occur in galaxies to link environment to morphology: strangulation, ram pressure stripping, and galaxy mergers.

1.2.1 Strangulation

Strangulation is the process by which a central late-type galaxy is deprived of its hot gas reservoir (Weinmann et al. 2006). This deprivation hinders the SFR over a long period of time, thus transforming into a galaxy with a low SFR, much like an early-type galaxy. Kawata & Mulchaey (2008) determine that the lack of hot gas in group environments is a plausible explanation for the higher SFR in groups than in clusters. Tanaka et al. (2004) touched on the effects of strangulation and galaxy-galaxy interactions as a means of transforming morphologies, as well. From a more up-to-date study, it is suggested that strangulation leads to a more dramatic increase in stellar mass than other possible mechanisms, and that the time scale for this process is on the order of four billion years (Peng, Miaolino, & Cochrane 2015). This long time scale is due to the fact that in the process of strangulation, the hot gas in a galaxy is still available even after the quenching of gas, thus allowing for continued star formation.

Figure 1.2 illustrates two separate processes, with strangulation shown in the bottom timeline (part **b**). Strangulation is also shown by Peng et al. to slightly increase stellar metallicity and stellar mass. It is known that although strangulation affects a galaxy's SFR, the

shape of a galaxy after undergoing this process does not change. In other words, a disk galaxy whose hot gas reservoir is depleted would remain a disk.

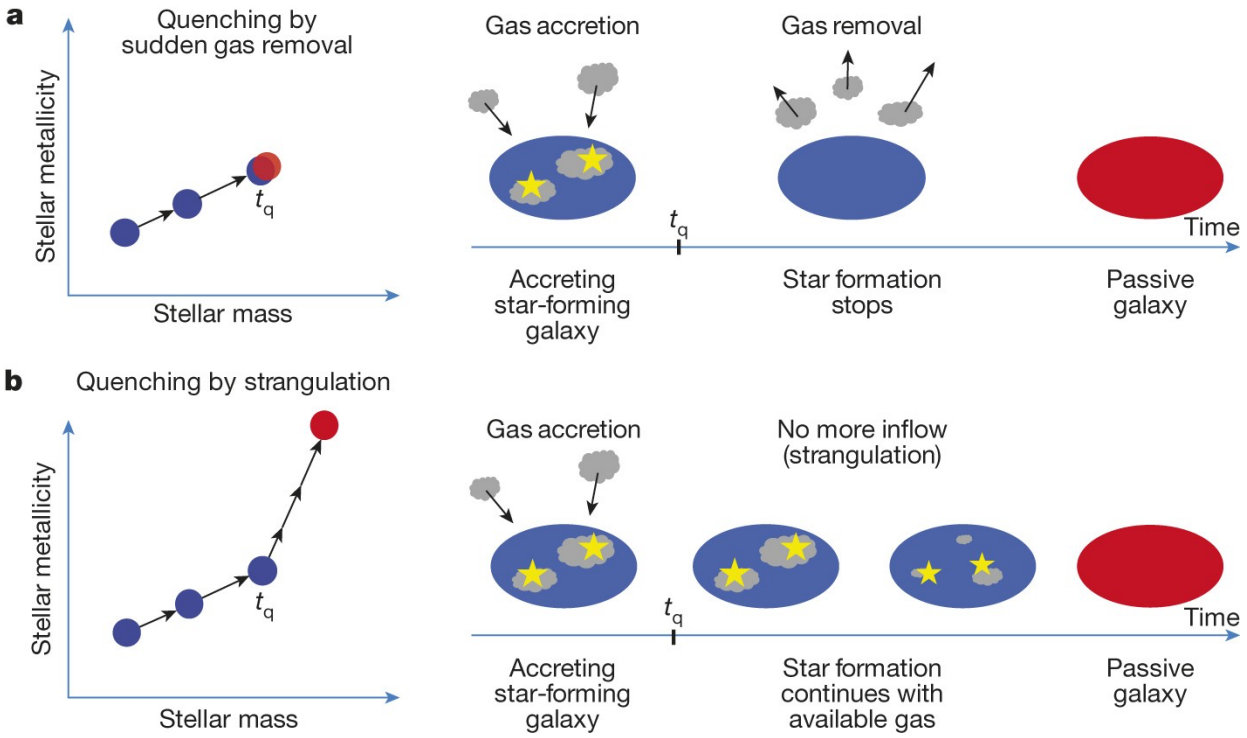

Figure 1.2. (Figure 1 from Peng, Miaolino & Cochrane (2015)) Illustration of **a**. The process of decreased star formation in a galaxy by the quenching of hot gas by sudden gas removal, i.e. ram pressure stripping (Section 1.2.2) and **b**. The process of decreased star formation in a galaxy by the quenching of hot gas by strangulation. t_q in the plots of stellar metallicity vs. stellar mass and on the timelines denote the quenching time. The red point in the plots represent the passive galaxy, or the galaxy after it has undergone each quenching process.

1.2.2 Ram Pressure Stripping

As a galaxy falls into a cluster or group's gravitational potential, a pressure is felt as it interacts with the intracluster medium known as the ram pressure (Karouzos, 2019). The ram pressure is given by

$$P_r \approx \rho_e v^2 \qquad (2)$$

where ρ_e is the density of the intracluster medium the galaxy interacts with and v is the velocity of the galaxy (Gunn & Gott, 1972). By balancing Equation 1 with the force per unit area needed for a typical disk galaxy to maintain its shape, Gunn & Gott (1972) concluded that if the density of the intracluster medium exceeds a particular threshold, then a galaxy will be stripped of its hot gas.

The process of ram pressure stripping is similar to strangulation in that it involves the depletion of the gas reservoir that is necessary for star formation (Weinmann et al. 2006). However, in ram pressure stripping, rather than the hot gas reservoir being simply depleted, all hot gas is removed from a galaxy, causing star formation to cease more closely to the quenching time. This process is illustrated in part **a** of Figure 1.2. As is seen in the plot of stellar metallicity vs. stellar mass, the passive galaxy has about the same metallicity and mass after undergoing ram pressure stripping. Similar to strangulation, the process of ram pressure stripping does not alter a galaxy's morphological shape. The main difference between ram pressure stripping and strangulation is the time scale. Strangulation generally takes much longer, and while there has been some debate on which time scale is more consistent with galaxy

evolution, Kauffman et al. (2004) and Peng et al. (2015) determined that the longer time scale is favored.

1.2.3 Galaxy Mergers

Galaxy mergers are largely held responsible for galactic evolution. There is significant evidence that mergers randomize the circular stellar orbits that exist within disk galaxies. This causes a disk galaxy to take on a more elliptical shape (Pearson, Wang, Alpaslan et al. 2019). Pearson et al. (2019) found that in the Sloan Digital Sky Survey (SDSS) catalogs, galaxies undergoing major merger events experienced a very slight increase in SFR (typically a factor of ~ 1.2). It is asserted that the SDSS catalogs provide a higher fraction of mergers among quiescent galaxies compared to star-forming galaxies, which implies that many of the mergers were likely gas-poor and therefore would not be able to boost SFR once merged. Before the Pearson et al. (2019) study, many studies suggested that galaxy mergers led to the quenching of star formation (Zepf & Ashman 1993; Moore, Katz, Lake et al. 1996). It has also been discussed that the cold disk gas of late-type galaxies could be driven to the galaxy's center, where the temperature drop could cause a starburst (Kodama, Smail, Nakata et al. 2001).

Schawinski et al. 2010 explores the effects of galaxy mergers on AGN, and relates the physical processes that occur to large-scale galaxy evolution. This study found substantial evidence that a major merger event resulted in an early-type spheroidal galaxy, and the timescale of a galaxy merger is on par with the observed Active Galactic Nuclei (AGN) processes.

Weinmann et al. (2006) discusses the merging of dark matter haloes in the 'nature scenario', and determines that galaxies closer to the halo center are more likely to merge. These collisions result in spheroid galaxies, and if gas is no longer accreted then the star formation rate will drop. This resulting galaxy will therefore be truly representative of an early-type galaxy in terms of both shape and star formation rate. However, if gas continues to accrete after the galaxy-galaxy collision, the spheroid shape will slowly transform back into a disk, representative of a late-type galaxy.

1.3 Application

The following provides background information on the catalogs and the instrument used for the purpose of this study. The group and galaxy catalogs from the SDSS Data Release 7 were used first to group low-redshift galaxies by their respective dark matter halos with specified halo masses. The Hyper-Suprime Cam Subaru Strategic Program is used for direct imaging of galaxies, and to collect properties such as galactic radius and Sérsic index. A galaxy's Sérsic index is its light profile modeled by the Sérsic function (Sérsic, 1963). The Sérsic function has become a popular method for modeling galactic light profiles by its generalization of the $R^{\frac{1}{4}}$ law to $R^{\frac{1}{n}}$, where n is the Sérsic index; $n = 4$ is indicative of luminous early-type galaxies (and sets the Sérsic function equal to de Vaucouleur's formula), whereas lower values of n such as $n = 1$ is indicative of late-type galaxies. The Sérsic function offers a nonparametric approach to modeling light profiles, which becomes necessary when describing a late-type galaxy's disk and

bulge components (see Pannella, Gabasch, Goranova et al. (2009) and included sources). For this experiment, we will consider Sérsic indices 0.3-2 to be late-type galaxies, and indices 2-8 to be early-type galaxies. For comparison of galaxies with different Sérsic indices, please refer to Figure 4 in section 3.2.

1.3.1 Yang et al. (2005) Group Catalog

The Yang et al. (2005) group catalog is a halo-based galaxy group finder that groups together galaxies residing in the same dark matter halo. This group catalog is an improvement from past group finders, and is reliable for poor systems such as small mass haloes. The catalog used in this report is from SDSS Data Release 7. A mass is assigned to each group that is used to estimate characteristics of the group, such as size and velocity dispersion (Yang, Mo, Van den Bosch et al. 2007). The absolute magnitudes of both the grouped galaxies and independent galaxies are found using the standard SDSS Petrosian technique (Yang, Mo, Van den Bosch et al. 2008). Because a galaxy is not a point source and rotates, different parts of the galaxy will appear at different redshifts and therefore different magnitudes; thus the correction of this phenomenon at a fixed aperture is necessary. The Petrosian technique accounts for this aperture correction (Petrosion 1976). In addition to using the Petrosian technique, the Yang et al. (2005) group catalog provides galactic magnitudes and colors that have been corrected for galactic extinction. For more information on the Yang et al. (2005) group catalog and the K-correction and evolution correction to redshift of 0.1, see Yang et al. (2008) and Blanton, Hogg, Brinkmann et al. (2003).

1.3.2 Hyper-Suprime Cam Subaru Strategic Program

The present study will use an extremely powerful instrument known as the Hyper-Suprime Cam Subaru Strategic Program (HSC-SSP) to observe galaxies in three different environments: halo mass less than 10^{13} solar mass (field regions), halo mass between 10^{13} and 10^{14} solar mass (groups of galaxies), and halo mass greater than 10^{14} solar mass (galaxy clusters).

The HSC-SSP is a deep, multi-band, three-layered imaging survey with an objective to provide clear images over a wide field of view to shed light on the gravitational weak lensing, galaxy evolution, supernovae, and galactic structure. This survey is carried out on the Subaru Telescope operated by the National Astronomical Observatory of Japan (NAOJ). The three layers of the HSC-SSP include the wide layer (1400 deg2), the deep layer (27 deg2), and the ultra-deep layer (3.5 deg2) (Miyazaki & Iwata 2014); the present study will focus on the wide layer (shown in the blue highlights of Figure 1.3). The combination of the wide field of view (1.7 degree diameter) HSC offers, and the large telescope aperture of the Subaru Telescope (8.2 meters) makes the HSC-SSP an extremely efficient survey instrument (Aihara, AlSayyad, Ando et al. 2019). The Subaru Telescope has a wider effective diameter than any of the telescopes that contribute to the SDSS, and so overcomes to the limitations of the latter survey (Gunn, Seigmund, & Mannery 2006; Bowen & Vaughan 1973; Holtzman, Harrison & Coughlin 2010).

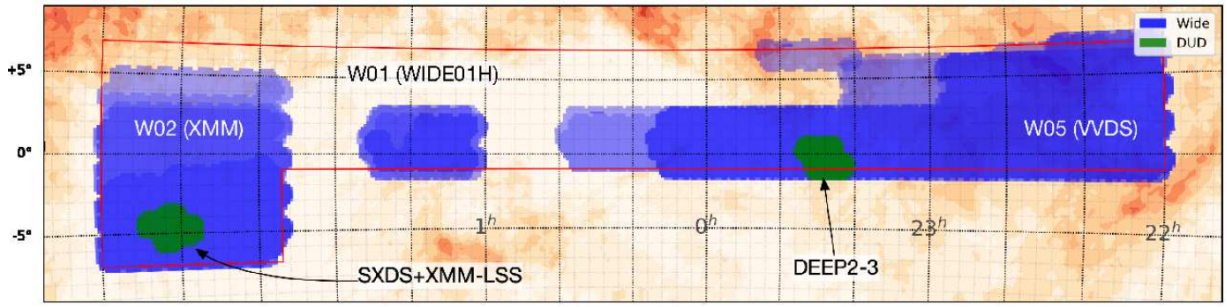

Figure 1.3. Map of HSC sky survey. The area in the Wide field is shown in blue, with the darker shades of blue indicating that the area is provided in more than one band up to the five available filters. The red boundary represents the limits of the Wide survey (Aihara, AlSayyad, Ando et al. 2019).

Prior to the commission of the HSC-SSP, the Suprime-Cam (otherwise known as the Subaru Prime Focus Camera) was a mosaic of ten CCD's on the Subaru Telescope (as opposed to the 104 CCD's of the HSC-SSP). Although the Suprime-Cam was decommissioned in 2017, the studies done using this camera (e.g. Kodama, Smail, and Nakata et. al 2001) were used to expand our understanding of galaxy evolution. Kodama et al. (2001) used the Suprime-Cam to study the distant rich cluster A851 at $z = 0.41$ to verify the observed bimodality of galaxy classification. This cluster allowed for a breakthrough in the discovery of the color-density relationship: it was previously known that blue (late-type) galaxies exist in low density regions, and red (early-type) galaxies exist in high-density regions; however, Kodama et al. (2001) discovered that the transition in the color-density behavior occurs in the 'subclumps' in the filaments surrounding the cluster. This identification could potentially lead to the determination of the nature of the relationship between galaxy morphology and environment. Because the transition occurs in

subclumps surrounding clusters, Kodama et al. (2001) may provide a better understanding of galaxy groups and their effects on galaxy morphology.

Further research has been done through the use of the HSC-SSP to determine the effect of environment on low surface brightness galaxies, which are defined as galaxies with central surface brightness being fainter than the night sky (Greco, Greene, Strauss et al. 2018). Greco et al. (2018) found that the surface brightness distribution depends strongly on color. Weak-lensing analysis has been performed on X-ray galaxy groups and clusters, and a concentration-mass relationship was established to work for both galaxy groups and clusters (Umetsu, Sereno, Lieu et al. 2020). However, Umetsu et al. (2020) used velocity dispersion in their calculations for halo mass, which Weinmann et al. (2006) argued to be less accurate than group luminosity.

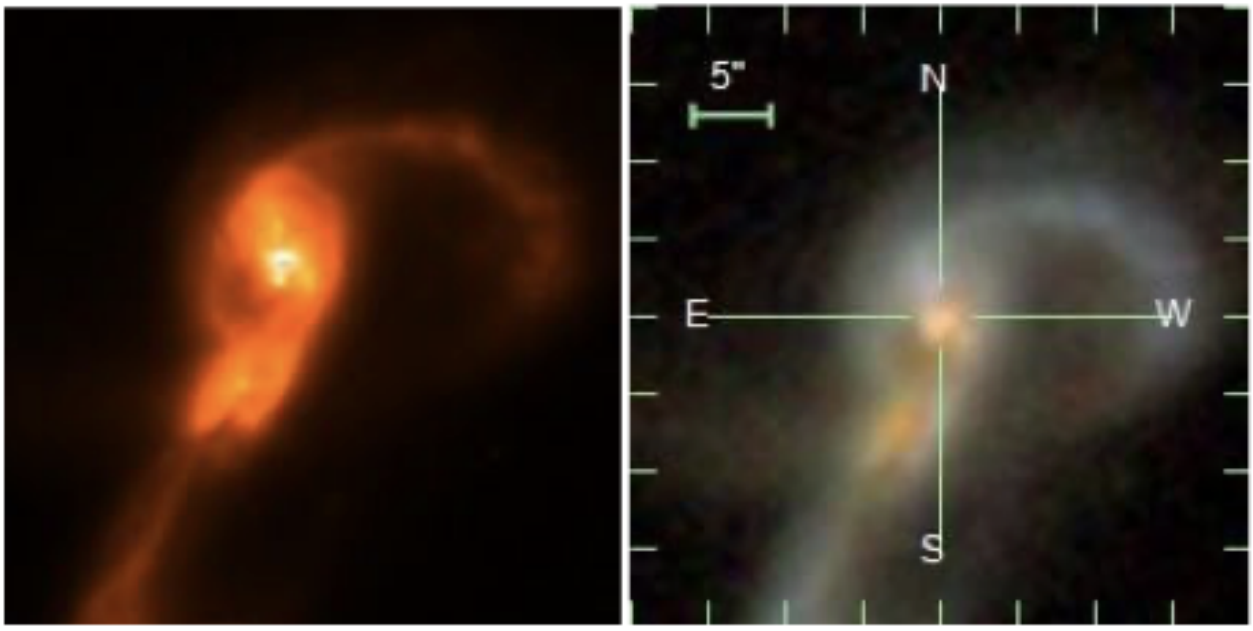

Figure 1.4. Side-by-side visualization of the same galaxy as seen from the HSC-SSP (left) and the SDSS (right). Based on the shape and tails of the object, it may be argued that this is a depiction of a galaxy merger.

Less studies have been conducted using the HSC-SSP on galaxy groups, particularly at low redshifts using the Yang et al. (2005) group catalog. Figure 1.4 shows one such galaxy as seen by the HSC instrument and the same galaxy as seen by the SDSS to illustrate the viewing capabilities of the HSC compared to previous surveys. The angular resolution of the HSC-SSP is evidently higher than the SDSS.

1.4 Thesis Objectives

Although the HSC-SSP has been employed in numerous studies surrounding galaxy clusters, more work needs to be done with the instrument to study groups of galaxies at low redshifts ($0.01 < z < 0.20$) using the Yang et al. (2005) group catalog. The present research project employs the strong observational capabilities of the HSC-SSP to study galaxy morphology in three different environments with the goal of determining how characteristics of galaxies change in the galactic field, groups, and clusters. The galaxy morphologies as quantified by the Sérsic index and SFR in each catalog will be plotted against stellar mass to investigate whether or not a correlation exists between mass and other properties.

The primary goals of this study are to (1) compare the morphological dependence of galaxies on environment at low redshifts using the Yang et al. (2005) catalog to previous studies, and (2) to determine the most probable mechanisms in clusters, groups and field regions that lead to the observed bimodality of galaxy morphology. This will hopefully improve astronomers' understanding of galaxy evolution.

Chapter 2

Data

2.1 Catalogs

Three catalogs of galaxies, groups, and clusters in these mass ranges were built using data from the Yang et al. (2005) group catalog and crossmatched with the HSC-SSP database.

2.1.1 Sloan Digital Sky Survey Data Release 7

The Sloan Digital Sky Survey (SDSS) is an extensive database that uses multi-color imaging and spectroscopy to create very detailed images and three dimensional maps of the universe. This report makes use of SDSS data release 7, built by Yang et al. (2005), specifically

based on the Petro magnitude as opposed to the model magnitude. The Petro catalogs hold group properties as well as individual galaxy properties.

The Petro group catalogs contain group IDs, Right Ascension (RA) and Declination (DEC), redshift, and halo mass as determined by luminosity. The Petro galaxy catalogs provide information about individual galaxies, such as galaxy ID and the group ID of the group they belong in.

2.1.2 GalSpecExtra-DR8

The GalSpecExtra-DR8 is a value added catalog of galactic properties made publicly available by the Max Planck Institute of Astrophysics and the John Hopkins University. This catalog is one of four that provides properties using spectra from SDSS data release 8. This is done using the GalSpec product (Kauffman, 2010). The GalSpecExtra model provides physical properties for each spectrum. For this study, this model is used to obtain star formation rate and stellar mass. This is done by using the three unique IDs given to each galaxy: PLATE ID, MJD ID, and FIBER ID.

2.1.3 HSC Database

Although the HSC-SSP is a multi-band imaging survey, this research will focus on the i-band images in the wide layer of the survey. Table 1 is taken from the HSC Available Data site, and shows quality of data in each layer and band.

Wide	g	r	i	z	y				
exposure (min)	10	10	16	20	16				
seeing (arcsec)	0.77	0.76	0.58	0.68	0.68				
depth (mag)	26.6	26.2	26.2	25.3	24.5				
saturation (mag)	17.6	17.4	18.0	17.5	17.3				
area (deg^2)	942	1022	796	905	924				
Deep+UltraDeep	g	r	i	z	y	$NB387$	$NB816$	$NB921$	$NB1010$
exposure (min)	49	45	65	130	88	68	120	112	—
seeing (arcsec)	0.81	0.74	0.62	0.63	0.71	0.80	0.69	0.66	—
depth (mag)	27.3	26.9	26.7	26.3	25.3	25.1	26.1	25.9	—
saturation (mag)	18.1	18.2	18.7	17.7	17.3	14.7	17.0	17.0	—
area (deg^2)	35	35	35	36	36	22	26	28	—
Wide									
target exposure (min)	10	10	20	20	20				
target depth (mag)	26.8	26.4	26.2	25.4	24.7				
Deep									
target exposure (min)	84	84	126	210	126	84	168	252	
target depth (mag)	27.8	27.4	27.1	26.6	25.6	24.8	26.1	25.9	
UltraDeep									
target exposure (min)	420	420	840	1134	1134		630	840	1050
target depth (mag)	28.4	28.0	27.7	27.1	26.6		26.8	26.5	25.1

Table 1. Taken from the HSC data release website, this table shows the capabilities of each HSC survey layer in each imaging band. This research focuses on the wide layer in the i-band.

2.2 Decomprofile Code

Published on GitHub, the Decomprofile code is a Python package that can be used to to model image data. This code makes use of Lenstronomy tools to create models of galaxy cutouts based on the 2D Sérsic light profile (Birrer & Amara 2018). The output of the Decomprofile code involves four main plots, including the raw data from the galaxy cutout, the model created by the code and Lenstronomy, a plot of the normalized residual for the model and data, and a plot showing goodness of fit based on the image and model pixels. Aside from the plots produced, the Decomprofile code also returns a JSON file for each galaxy. These JSON files contain unique information regarding the galaxy's properties, including Sérsic index, radius, magnitude, and amplitude.

Chapter 3

Methods

3.1 Catalog Matching

The first step in creating galaxy catalogs for the three environments is to divide the SDSS data release 7 Petro group catalogs into three halo masses. This was accomplished with simple AWK commands to filter the halo masses to be greater than 10^{14} solar masses for the cluster catalog, between 10^{13} and 10^{14} solar masses for the group catalog, and less than 10^{13} solar masses for the field catalog. These three catalogs will then be matched to the Petro galaxy catalogs with the group IDs, which is done using TOPCAT (Tool for OPerations on Catalogs And Tables). TOPCAT is a powerful tool used in astrophysics to read through tabular data. The Petro group catalog will provide columns with group ID, group RA, group DEC, group redshift, and halo mass. The Petro galaxy catalog will provide galaxy ID.

The next catalog to be matched with is the SDSS data release 7 with file name SDSS7. Galaxy IDs will be matched to obtain galaxy RA, galaxy DEC, and galaxy redshift. There is also a separate ID provided as the NYU ID; this is necessary in matching to the SDSS7_ID catalog. The NYU ID stems from the New York University Value-Added Galaxy Catalog (Blanton, Schlegel, Strauss, et al. 2005), and provides spectroscopic information on low redshift galaxies in the SDSS. The file SDSS7_ID will then be matched to by NYU ID to obtain three unique IDs known as PLATE ID, MJD ID and FIBER ID. These three IDs are necessary in matching to the GalSpecExtra-DR8 catalog.

By writing a Perl script to match the catalog thus far to the GalSpecExtra-DR8 catalog, the galaxies were matched through the PLATE ID, MJD ID and FIBER ID. Some galaxies had these three IDs equal to -1, which were taken to be unavailable in the Yang et al. (2005) group catalog. The Perl script was written to omit these particular galaxies. Furthermore, when a halo mass is too small to be assigned an accurate mass number, the Yang et al. (2005) catalog assigns these to have halo mass of zero. The Perl script also omitted these galaxies. The Perl script then printed out a complete catalog, and was altered to create each catalog of the three environments. The final catalogs contain group ID, group RA, group DEC, group redshift, halo mass, galaxy ID, galaxy RA, galaxy DEC, and galaxy redshift. Figure 2.1 shows a schematic of the catalog constructing process.

The three catalogs are then cross-matched to the HSC-SSP database by using the HSC matching script provided on GitLab. This script is run through Python and uses the positions of galaxies to determine the available galaxies in the HSC database.

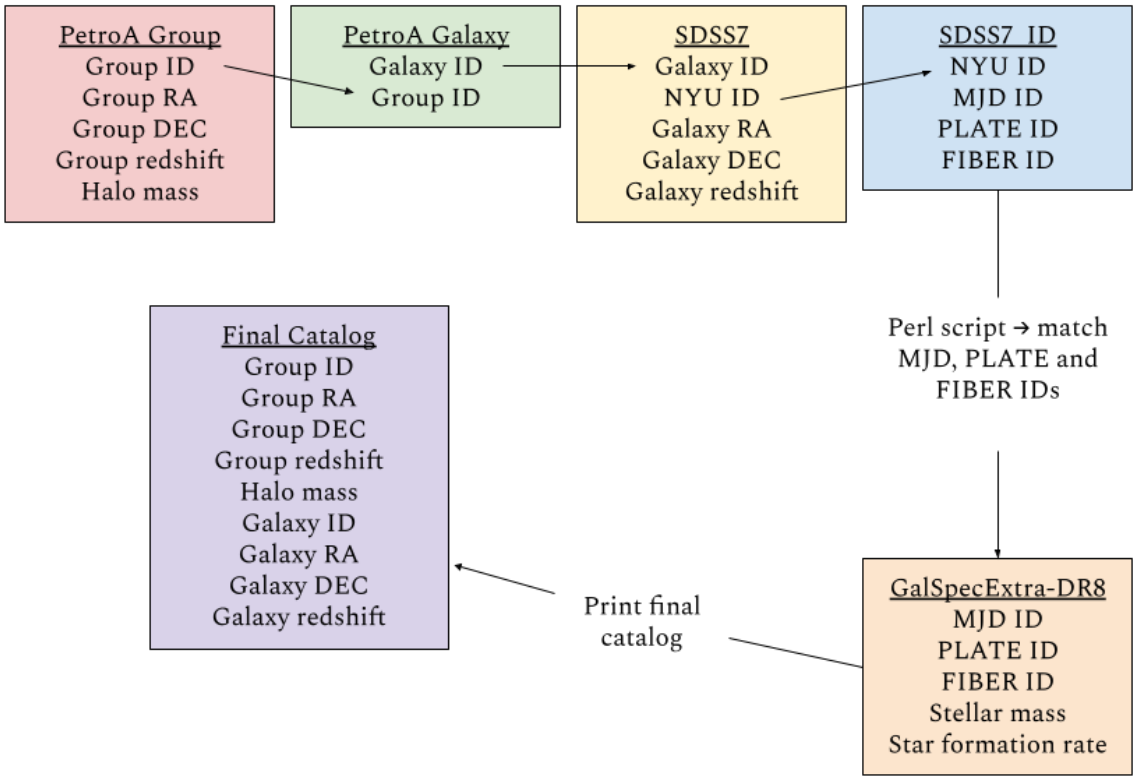

Figure 2.1. Schematic of the catalog constructing process, showing relevant column data of each SDSS catalog used in creating the final catalog. The starting catalog (PetroA Group) will have specified halo mass according to the chosen regimes of clusters, groups and fields set by AWK commands.

3.2 Galaxy Cutouts

The cutout tool produced two .fits files for each galaxy, one of which was the image cutout of the galaxy and the other was the modeled point-spread function (PSF) file. This cutout tool is provided in the Public Data Release 2 of HSC imaging. Figure 2.2 shows an example of eight galaxy cutouts as seen in the SAO Image DS9 software, which is a visualization tool used

to view astronomical data. The galaxies shown have Sérsic indices from one to eight to show the evolving shapes as Sérsic index changes. At the low Sérsic index of one (n = 1, where n is Sérsic index), the galaxy clearly takes on a long disk-shape. The orientation of the galaxy matters in the case of viewing it's disk structure, and several studies (e.g. Weinmann et al. (2006)) address the effect viewing orientation has on a galaxy's classification. For galaxies with high Sérsic index (n = 8), it is clear that the galaxy is more spheroidal in shape. This evolution from disk to elliptical is seen throughout the eight cutouts in Figure 2.2.

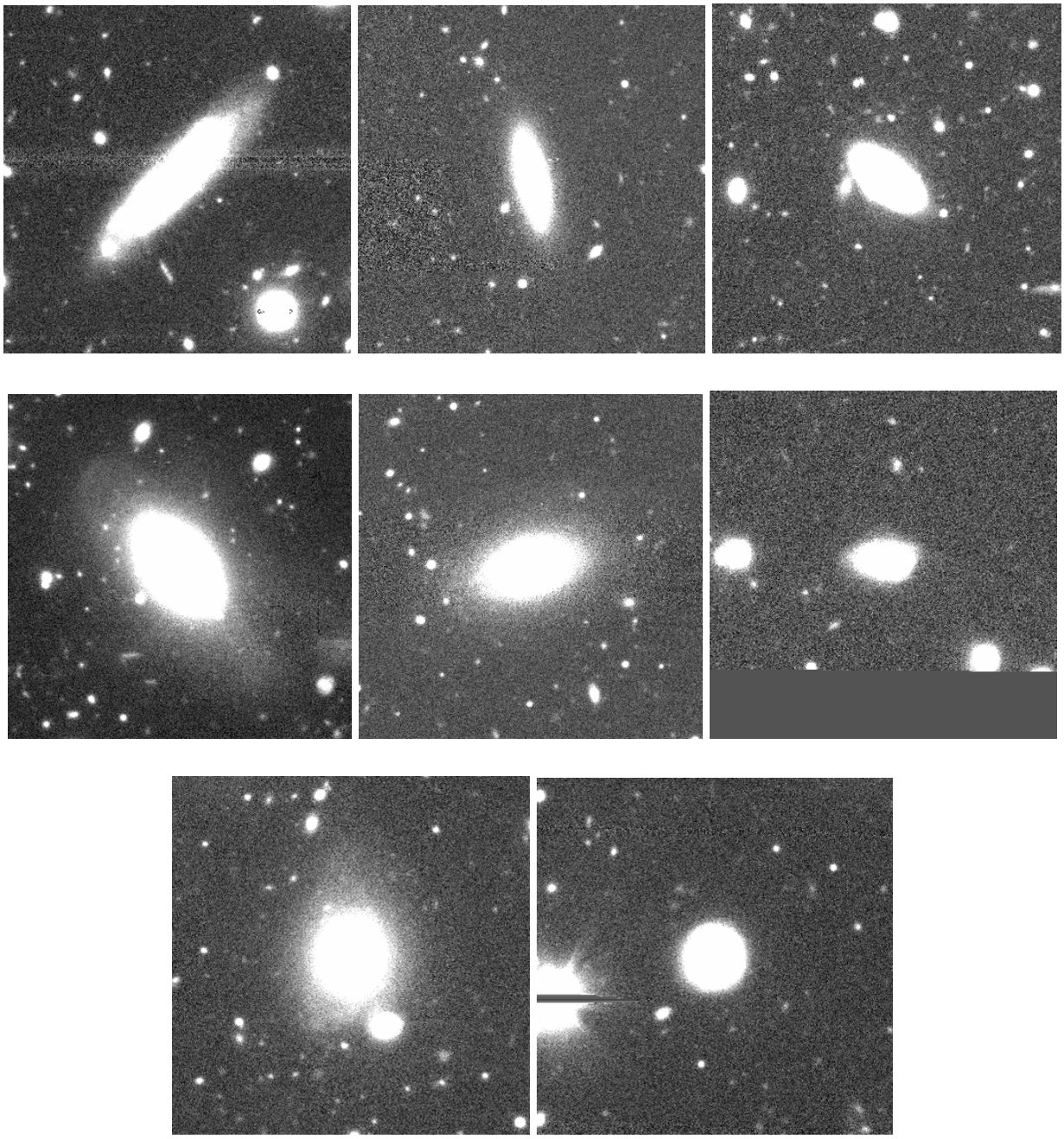

Figure 2.2. From left to right and top to bottom, images of galaxies with increasing Sérsic index are shown from $n = 1$ to $n = 8$. These images are direct galaxy cutouts from the HSC Public Data Release 2 cutout tool, and have been rendered for viewing in the SAO Image DS9 software, viewed on a linear scale in greyscale.

3.3 Decomprofile Code

After galaxy cutouts and point-spread function (PSF) files were created for galaxies in the three catalogs, it was time to extract information on morphological properties of each galaxy. This was done using the Decomprofile code available on GitHub. Because the Decomprofile code is designed to run only one galaxy at a time, a Perl script was written to run the code in batch mode on all available galaxy cutouts and associated PSF files.

At the conclusion of running all three directories of cutouts through the Decomprofile code, we were left with a total of 254 galaxies in clusters, 3,726 galaxies in groups, and 5,496 galaxies in field regions. For each galaxy, the Decomprofile code output a PDF file containing four plots: the data image of the galaxy cutout, the light profile model created by the code, the normalized residual plot of the model and data, and a plot of the goodness of fit of the Decomprofile model along with its residual plot. Figure 3.1 shows an example of a PDF file. Along with the PDF, a JSON file was produced for each galaxy that communicated several properties of each galaxy, including Sérsic index and radius.

Although the Decomprofile code was able to successfully model and produce data for most of the galaxy sample, a small fraction of galaxies appeared to have Sérsic indices too high to be consistent with the rest of the data. A plot of Sérsic index as a function of stellar mass is shown in Figure 3.2, where galaxies (of all masses) appear to have a high Sérsic index of around 9. It was concluded that the Decomprofile code was not able to successfully fit the light profiles of these galaxies due to the boundary of Sérsic index being exceeded. For time's sake, we were unable to investigate the reason behind the Decomprofile code's shortcomings further, but

omitted these galaxies from all three catalogs. As a result, the final count for galaxies in the three environments are as follows: 5239 galaxies in the field region; 3575 galaxies in groups; and 234 galaxies in clusters.

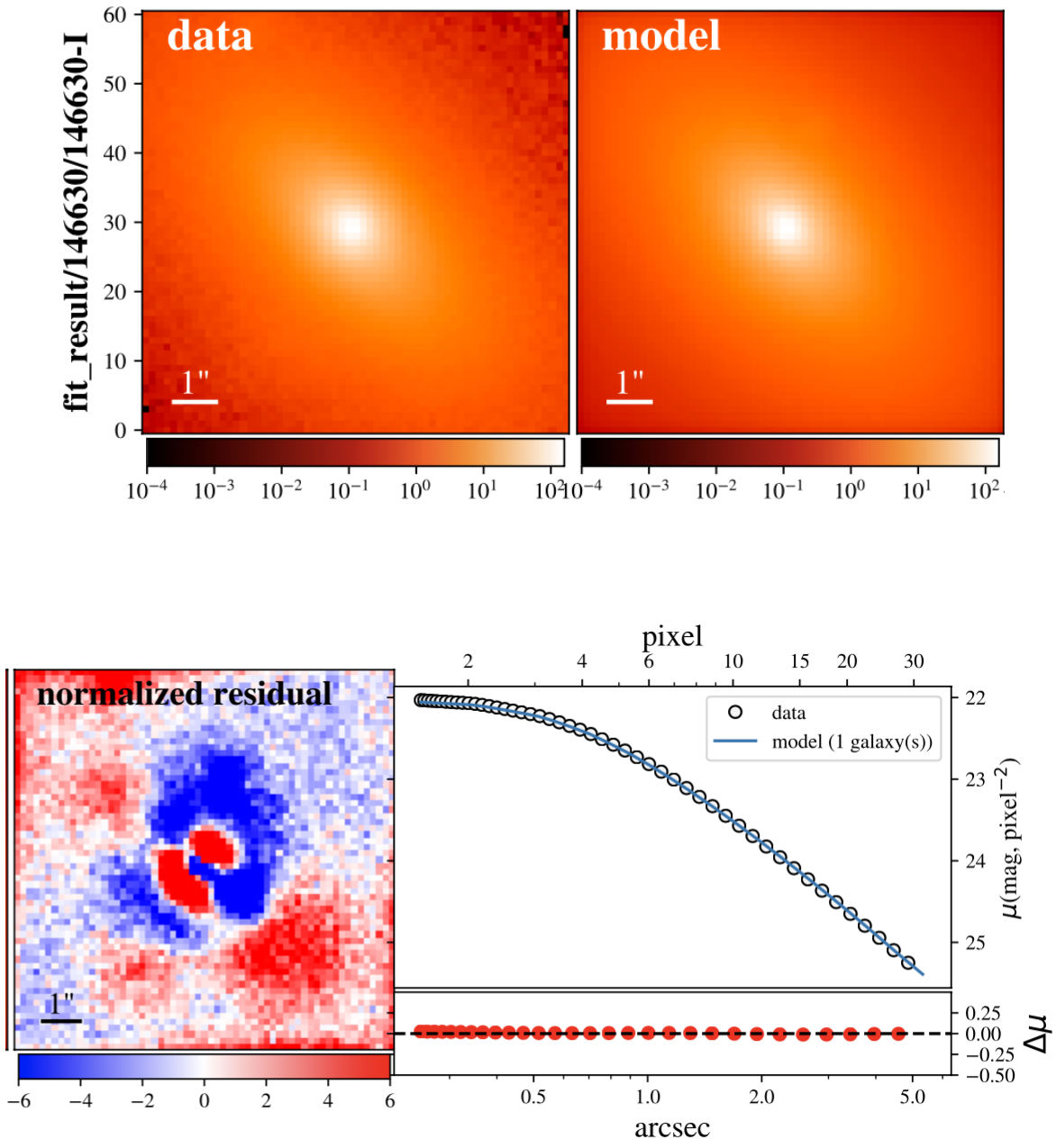

Figure 3.1. Example of Decomprofile code output for galaxy with ID 146630. From left to right and top to bottom, plots produced are data from galaxy cutout, a model of the light profile created by the Decomprofile code, the normalized residual of the model and data, and the goodness of fit plot, where residual plot is shown below.

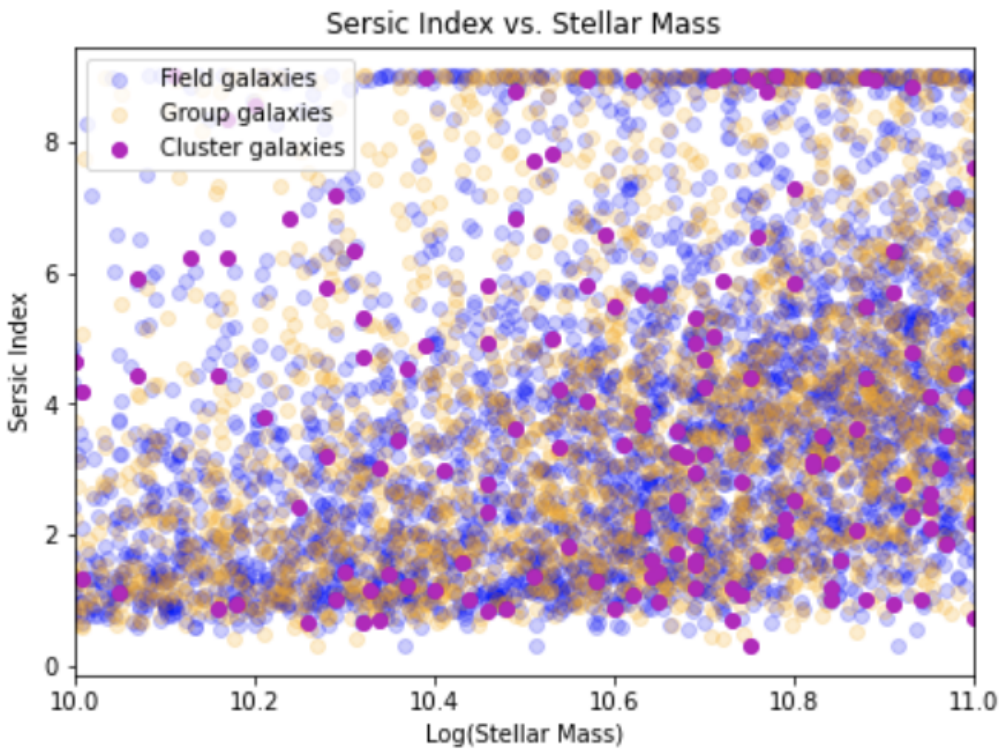

Figure 3.2. Plot of Sérsic index vs. log of stellar mass. Note that around Sérsic index 8.95, there are many galaxies in the field, groups and clusters. This disrupts the trend seen in the rest of the plot, as well as exceeds the Sérsic index range. These galaxies are results of failure in fitting light profiles by the Decomprofile code, and will not be included in the results of this report.

The last step of catalog construction was to match the final catalogs for each environment to print only the galaxies that were made available by the cutout tool.

3.4 Python Code

After models were created and data of galactic properties were extracted using the Decomprofile code, a Python script was constructed to work with data in the produced directories containing the JSON files, as well as loading the catalogs for each environment. Plots were then created to show correlation between various galactic properties. An important property of galaxies is the distance from the dark matter halo's center, which required calculating projected distances from RA and DEC.

3.4.1 Calculating Projected Distances

The Decomprofile code output galaxy radii in units of arcseconds, which needed to be converted to kiloparsecs for further calculation. This was done through use of tools from the Astropy package, specifically the Cosmological Calculations sub-package (otherwise known as astropy.cosmology). By using the redshift of galaxies as obtained from SDSS catalogs, the Cosmology sub-package's FlatLambdaCDM tool calculated distance in kpc/arcmin. The platescale was then calculated by dividing this value by 60, essentially converting the distance to units of kpc/arcsec. By multiplying the platescale by the list of galactic radii for each galaxy in the three halo mass environments, the radius was calculated in units of kiloparsecs.

A factor studied in this paper is a galaxy's distance from its dark matter halo's center. Although the RA and DEC of both the individual galaxies and haloes are provided by the SDSS

catalogs, it was necessary to convert these coordinates to projected distances between objects in kiloparsecs. This was done using the Cosmology sub-package's tool to calculate distances between two objects in three-dimensional space.

3.4.2 Creating Indices for Measured Properties

In order to better understand galaxy morphology, it is helpful to observe trends of certain galactic properties in terms of others. For example, by dividing galaxies into star-forming (logarithmic SFR > 0) and quiescent (logarithmic SFR < 0), we can see the fraction of each classification that are disk-shaped as opposed to ellipticals. This is done by using the simple `numpy.where` method, which returns elements from a specified list depending on a given condition. This method is used to create indices for SFR, Sérsic index, and stellar mass.

Chapter 4

Results

4.1 Stellar Mass vs. Redshift

To answer the question of environmental dependence on galaxy morphology, the first step is to establish a range of stellar mass that is representative of galaxies in the three environments. Figure 4.1 below shows the plots of galactic stellar mass as a function of redshift for all data points and for points in the range log(10) - log(11) solar mass.

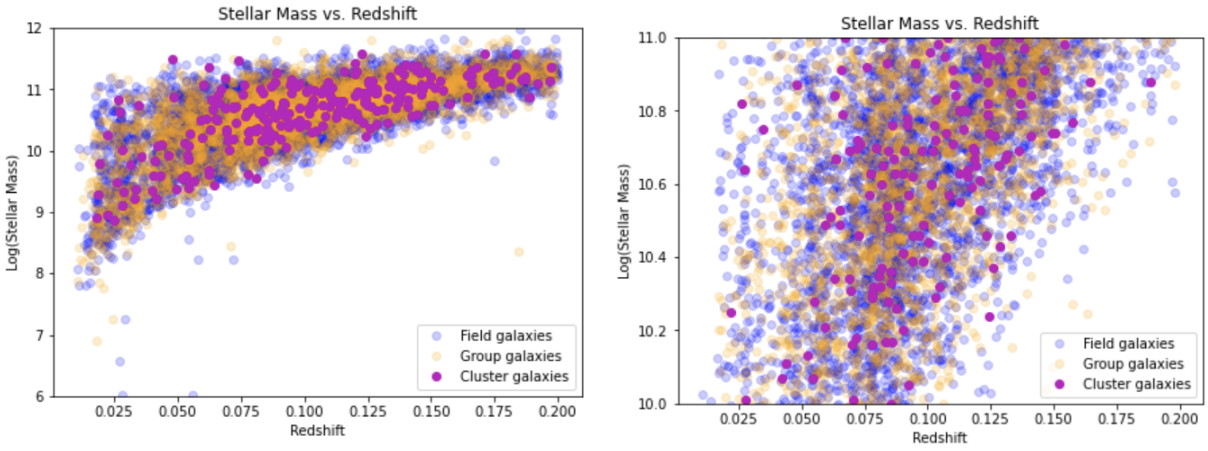

Figure 4.1. Plots of the log of the stellar mass vs. galactic redshift, and the same plot in log of stellar mass range 10 - 11. Galaxies in the three environments are divided by color: field galaxies in blue, galaxies in groups are orange, and cluster galaxies in magenta. This color coding will be consistent with all following plots and histograms.

4.2 Star Formation Rate

4.2.1 SFR vs. Stellar Mass

As is made clear in previous studies (i.e. Naab, Khochfar, & Burkert 2006), SFR is often indicative of galaxy classification. In order to observe trends in SFR and environment in the created catalogs, a log-log plot of SFR as a function of stellar mass is shown in Figure 4.2 (below). It is clear that the galaxies in the field region (shown in blue) tend to have higher SFR

than the cluster or group galaxies (in magenta and orange, respectively). This is seen specifically when the log of SFR is equal to one. At the lower limit of SFR, however, quiescent galaxies (as opposed to star-forming galaxies) occupy cluster and field environments. There is also a clear correlation between stellar mass and SFR in Figure 4.2, as there is an increase in SFR as the log of the stellar mass increases. This relationship is seen predominantly in field and group galaxies, while galaxies in clusters exhibit steady SFR at or below 10 solar masses per year.

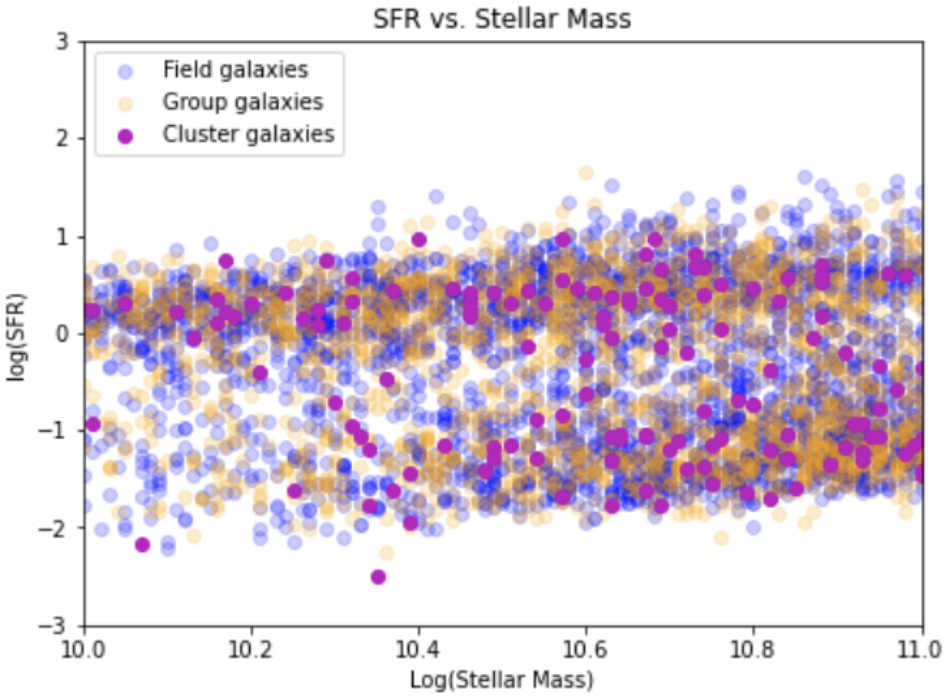

Figure 4.2. Plot of logarithmic SFR vs. logarithmic stellar mass.

4.2.2 Histograms of SFR in Stellar Mass Ranges

Within the stellar mass range of log(10) - log(11), three stellar mass bins were created to depict galactic properties in a low stellar mass range (log(10) - log(10.333)), a mid stellar mass range (log(10.333) - log(10.666)), and a high stellar mass range (log(10.666) - log(11)). Histograms of the SFR of galaxies in these three stellar mass bins is shown in Figure 4.3. The average SFR in each of the bins and for each of the environments is printed below the plots. All histograms are normalized by setting `density=True` in the matplotlib Python package, which essentially sets the area beneath the histogram bars equal to one. In the mid and high stellar mass ranges, the average SFR is highest in the field region and lowest in galaxy clusters; however, the opposite is true for the low stellar mass range.

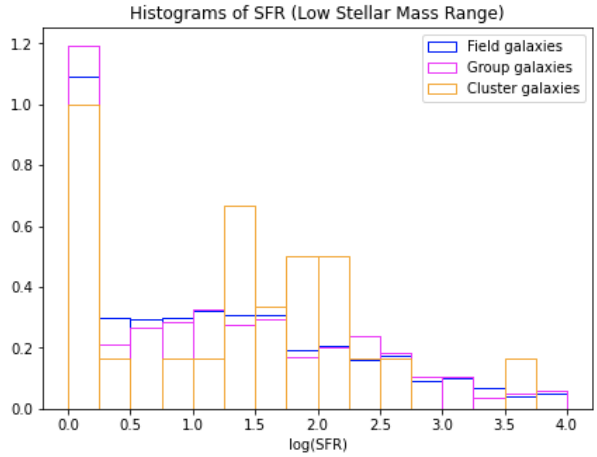

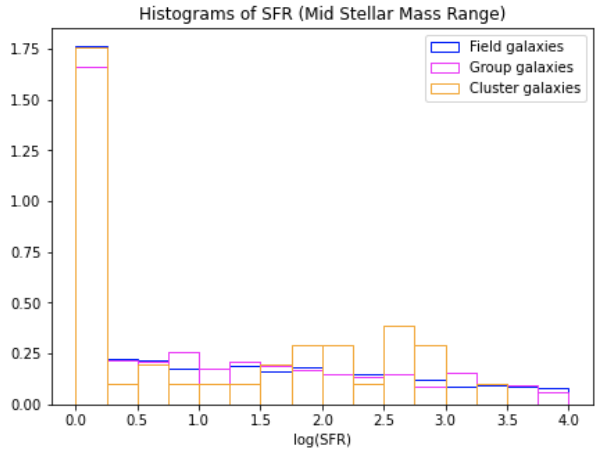


```
Average SFR (field) =  1.36
Average SFR (group) =  1.4
Average SFR (clust) =  1.65
```

```
Average SFR (field) =  1.89
Average SFR (group) =  1.88
Average SFR (clust) =  1.53
```

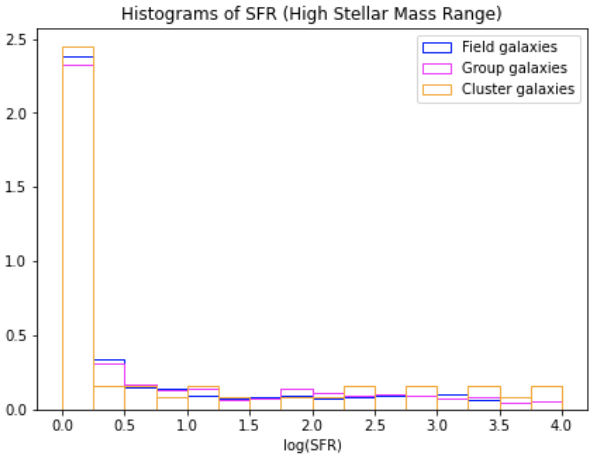


```
Average SFR (field) =  2.04
Average SFR (group) =  1.75
Average SFR (clust) =  1.53
```

Figure 4.3. Three normalized histograms of SFR in three stellar mass indexes: low (top left), mid (top right), and high (bottom). Average SFR for each environment and stellar mass bin is printed.

4.2.3 Histograms of SFR in Late- and Early-Type Galaxies

Similar to creating stellar mass bins to depict galactic properties, Sérsic index was indexed by two bins: late-type galaxies (Sérsic index less than 2) and early-type galaxies (Sérsic index greater than 2). Histograms of SFR in these two bins are shown in Figure 4.4 (below). In all environments, the SFR is higher in late-type galaxies, and decreases as environmental density increases. It is clear from the histogram shapes that a significant amount of early-type galaxies have low SFR, whereas the SFR in late-type galaxies ranges from zero to four, and the drop is more gradual.

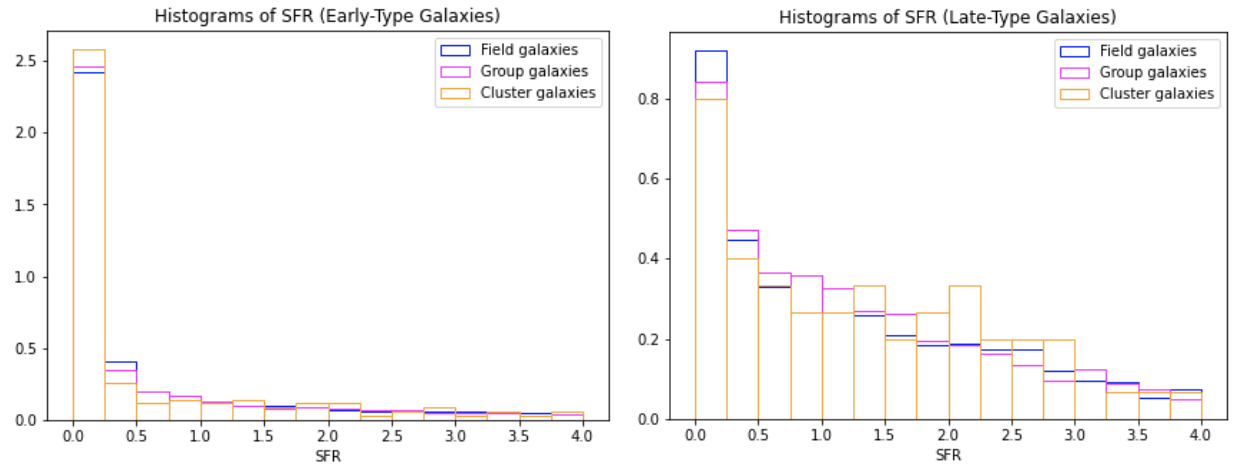


```
Average SFR (field) =  1.43
Average SFR (group) =  1.24
Average SFR (clust) =  0.92
```

```
Average SFR (field) =  2.23
Average SFR (group) =  2.05
Average SFR (clust) =  2.07
```

Figure 4.4. Normalized histograms of SFR in early-type (left) and late-type galaxies (right) with averages printed for each environment.

4.3 Sérsic Index

4.3.1 Sérsic Index vs. Stellar Mass

One of the most telling characteristics of a galaxy's morphological type is its shape parameter. The plot shown in Figure 4.5 (below) shows Sérsic index as a function of stellar mass in the appropriate stellar mass range. Although a clear trend is hard to decipher from this plot, it can be argued that a slight upward trend can be observed in the field region as stellar mass increases, which would imply that more massive galaxies tend to have a more elliptical shape. Cluster galaxies, on the other hand, are fairly evenly distributed throughout all stellar masses, and make appearances as both disk and elliptical galaxies.

The build-up of galaxies seen in the upper region of the plot at Sérsic index = 10 indicates a problem with the Decomprofile code and its ability to read some galactic light profiles.

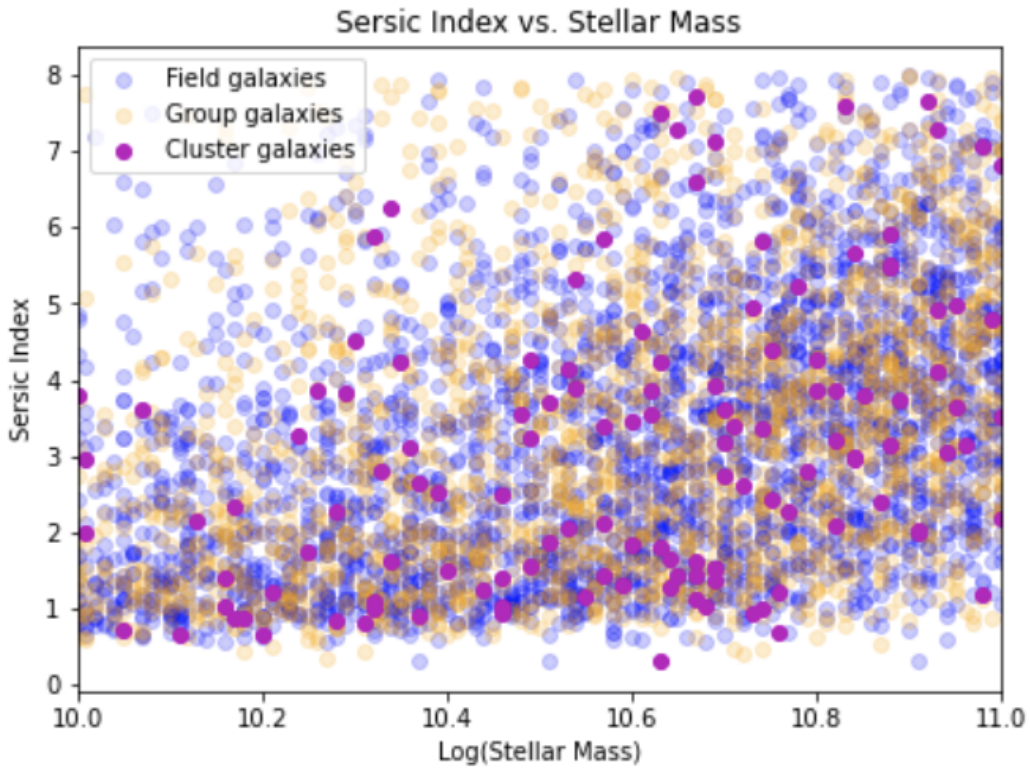

Figure 4.5. Plot of Sérsic index vs. log of stellar mass.

4.3.2 Histograms of Sérsic Index in Stellar Mass Bins

Figure 4.6 (below) shows the histograms of Sérsic index in the three stellar mass bins. In all stellar mass ranges, Sérsic index appears to decrease as halo mass increases. In the high stellar mass range, galaxies in groups have an average Sérsic index of 3.88, which acts as a transition between the field galaxy average (3.9) and the cluster galaxy average (3.65). This behavior is not observed in the low or mid stellar mass bins, which report average Sérsic index to

be highest in galaxy groups. It can be seen that galaxies with the highest stellar masses have higher average Sérsic indices, and the peak of all three environments is higher than the positions seen in the low and mid stellar mass ranges. This leads to the conclusion that elliptical galaxies are more massive than disk galaxies. It can also be seen that the transition from disks to ellipticals is much more gradual in high-mass galaxies, whereas the decline is very steep in the low- and mid-mass galaxies.

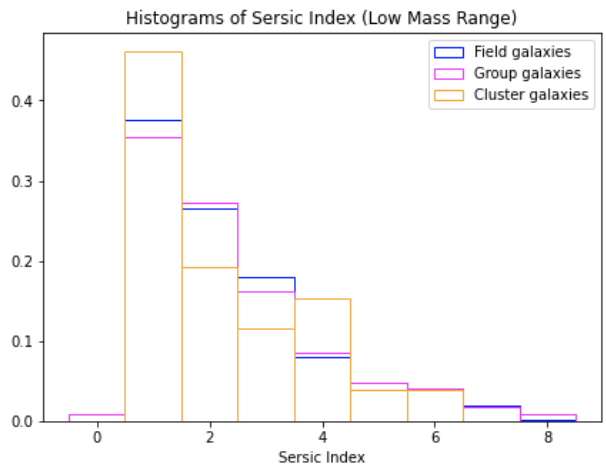

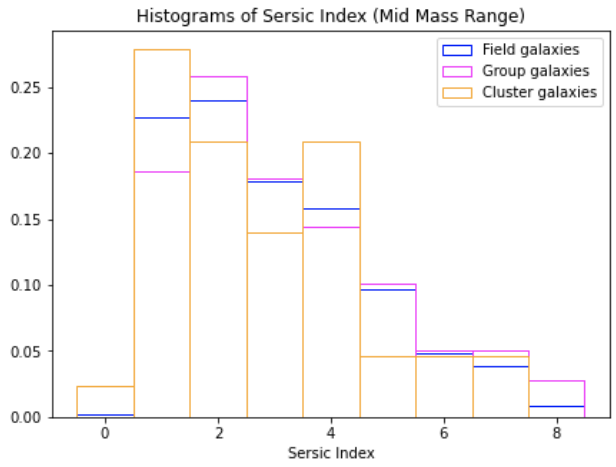


```
Average sersic index (field) =  2.35
Average sersic index (group) =  2.43
Average sersic index (clust) =  2.16
```

```
Average sersic index (field) =  3.01
Average sersic index (group) =  3.18
Average sersic index (clust) =  2.85
```

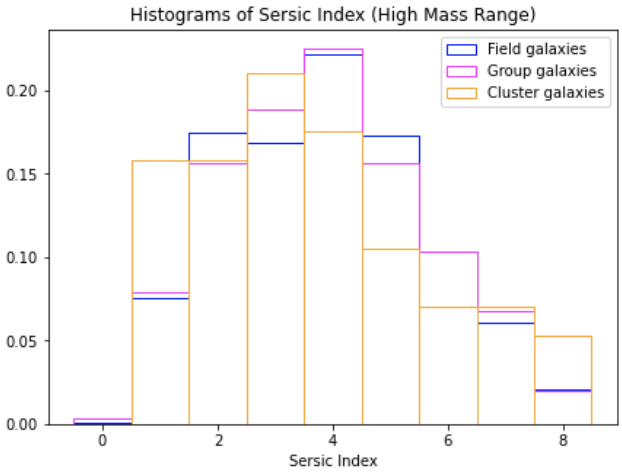


```
Average sersic index (field) =  3.9
Average sersic index (group) =  3.88
Average sersic index (clust) =  3.65
```

Figure 4.6. Normalized histograms of Sérsic Index in stellar mass bins: low (top left), mid (top right), and high stellar mass (bottom). Average Sérsic index is printed for each environment in all stellar mass bins.

4.3.3 Histograms of Sérsic Index in Star-Forming and Quiescent Galaxies

SFR was broken into two bins: star-forming galaxies with log(SFR) greater than zero, and quiescent galaxies with log(SFR) less than zero. This was done so that galactic properties could be shown in relation to the star-forming tendencies of individual galaxies in the different environments. Figure 4.7 (below) shows Sérsic index histograms in these two SFR bins, and include the printed average Sérsic indices in each environment. It app;ears that in both bins, there is little noticeable effect on Sérsic index. However, it is observed that quiescent galaxies have a higher average Sérsic index in all environments, meaning that quiescent galaxies are more often elliptical.

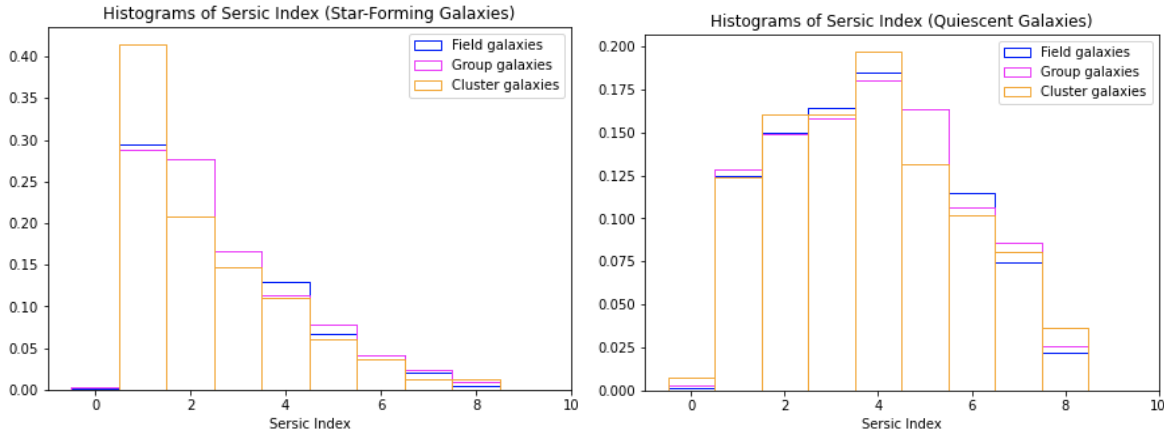


```
Average sersic index (field) =  2.63
Average sersic index (group) =  2.67
Average sersic index (clust) =  2.42
```

```
Average sersic index (field) =  3.86
Average sersic index (group) =  3.88
Average sersic index (clust) =  3.82
```

Figure 4.7. Normalized histograms of Sérsic index in star-forming (left) and quiescent (right) galaxies.

4.3.4 Sérsic Index vs. Stellar Mass in Star-Forming and Quiescent Galaxies

In order to visualize the relationship between Sérsic index and stellar mass in bins of star-forming and quiescent galaxies, the plots shown in Figure 4.8 (below) were created. There is a clearer upward trend of Sérsic index for both field and group galaxies in the quiescent bin, while the cluster galaxies show a fairly even distribution throughout the stellar mass range. In both plots, the upward trend with stellar mass is prevalent in field and group galaxies, meaning that more massive galaxies in less dense environments are elliptical-shaped regardless of their status as star-forming or quiescent. However, low-mass star-forming galaxies tend to take on a disk shape more readily than low-mass quiescent galaxies.

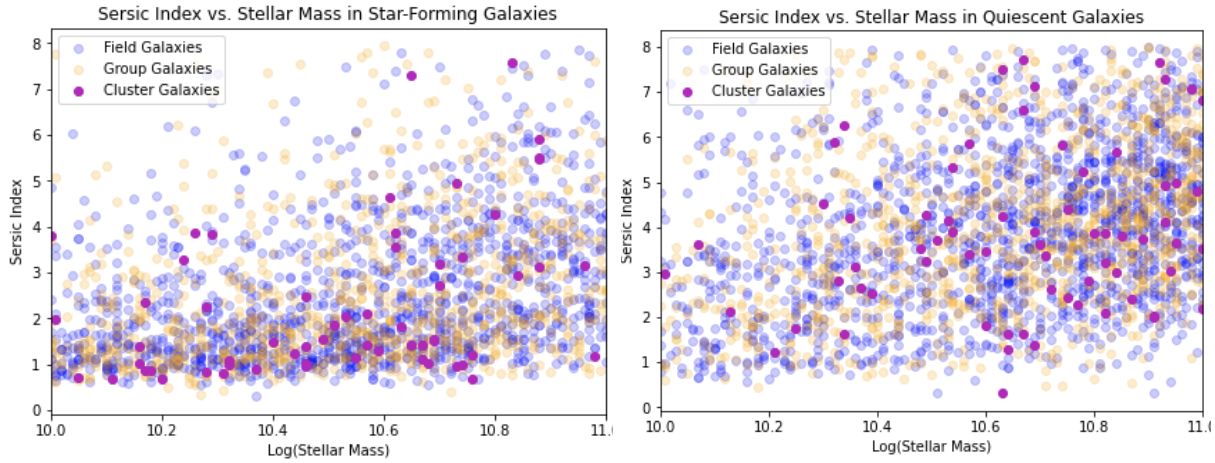

Figure 4.8. Plots of Sérsic index vs. the log of the stellar mass in star-forming galaxies (left) and quiescent galaxies (right).

4.4 Radius

4.4.1 Radius vs. Stellar Mass

The plot shown in Figure 4.9 (below) shows the plot of logarithmic radius in kiloparsecs as a function of the logarithmic stellar mass. The size of a galaxy has shown correlation with galactic morphology in previous studies, and the following plot shows field galaxies having larger radii than group and cluster galaxies. From Figure 4.9, it can be seen that galaxies with higher stellar mass are larger in size.

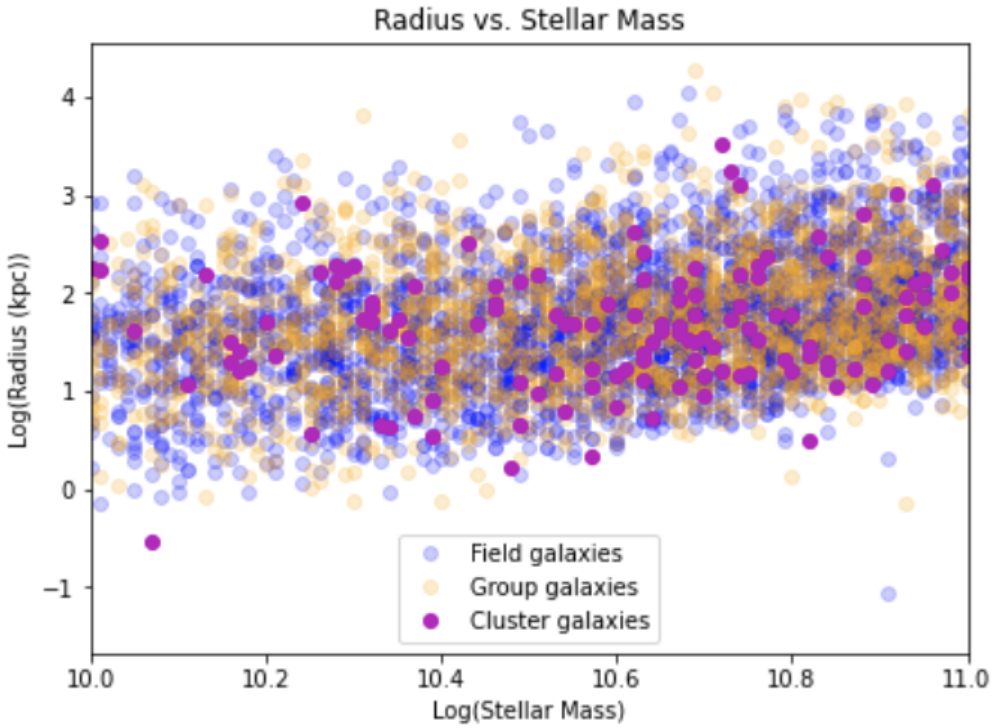

Figure 4.9. Plot of log of radius (kpc) vs. the log of the stellar mass.

4.4.2 Histograms of Radius in Stellar Mass Bins

In Figure 4.10 (below) are the histograms of logarithmic radius in three different stellar mass bins. It is clear from the printed averages of galactic radius in the three stellar mass ranges that more massive galaxies are larger in size. In clusters, note that the trend in radius is not a

steady increase as stellar mass increases; the average size of mid-stellar mass galaxies in clusters is smaller than that of low-stellar mass galaxies in clusters.

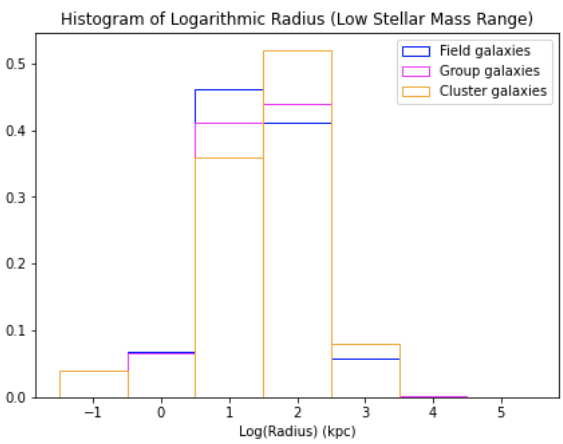

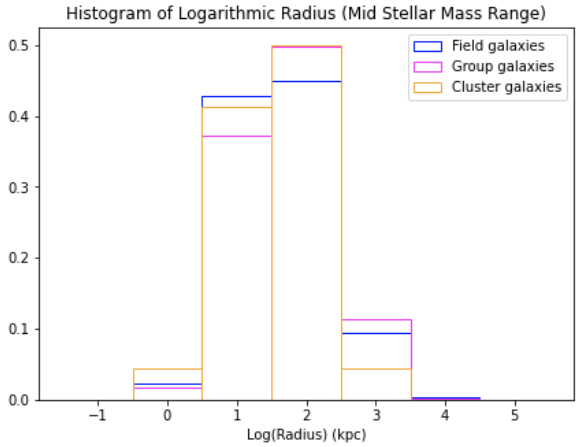


```
Average log(radius) (kpc) (field) =  1.46 Average log(radius) (kpc) (field) =  1.62
Average log(radius) (kpc) (group) =  1.53 Average log(radius) (kpc) (group) =  1.7
Average log(radius) (kpc) (clust) =  1.65 Average log(radius) (kpc) (clust) =  1.46
```

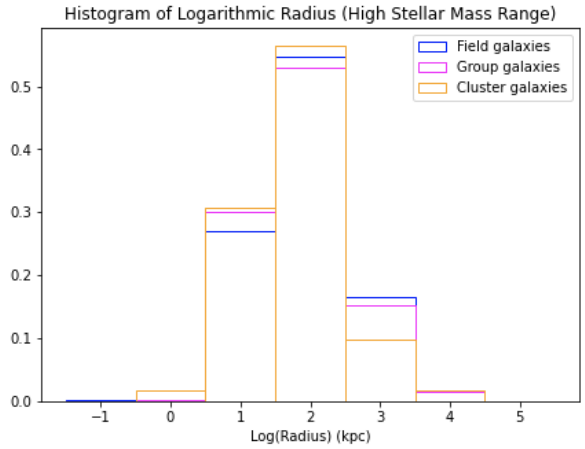


```
Average log(radius) (kpc) (field) =  1.93
Average log(radius) (kpc) (group) =  1.9
Average log(radius) (kpc) (clust) =  1.82
```

Figure 4.10. Three normalized histograms of logarithmic radius in stellar mass bins: low (top left), mid (top right), and high stellar mass range (bottom). Average log(radius) in kpc is printed for each environment in the three stellar mass bins.

4.4.3 Histograms of Radius in Star-Forming and Quiescent Galaxies

Figure 4.11 (below) shows histograms of radius in the two previously defined SFR bins, labeled star-forming galaxies and quiescent galaxies. Viewing galactic size in these bins reveals a possible correlation in the lower density regions. Star-forming galaxies in the field region are larger on average than quiescent galaxies in the field, and the same can be said for galaxies in groups and in clusters.

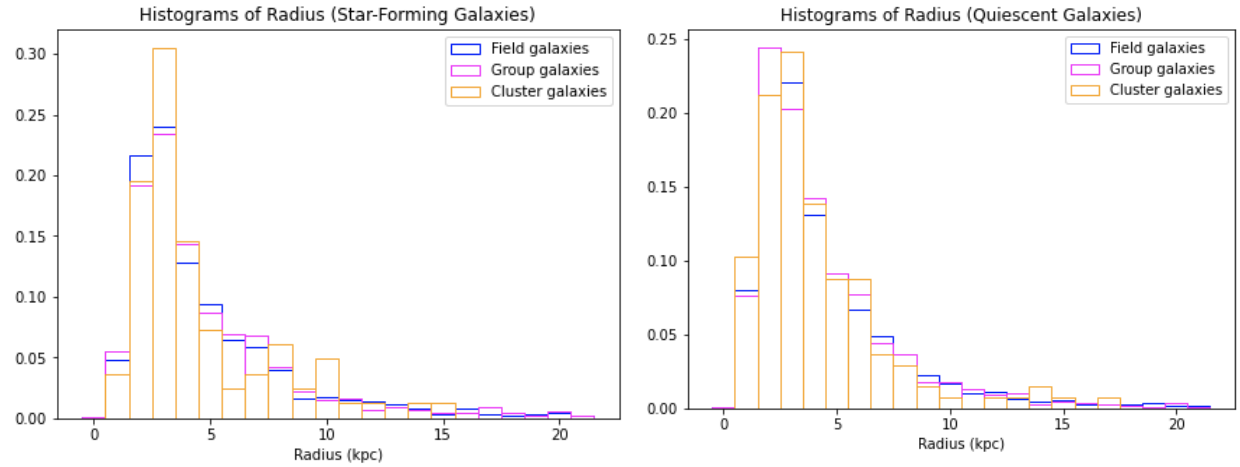

Figure 4.11. Normalized histograms of galactic radii in star-forming (left) and quiescent (right) galaxies with average radius in kpc printed for each environment.

4.4.4 Histograms of Radius in Early- and Late-Type Galaxies

Radius was also observed in the two separate indices based on Sérsic index: late-type galaxies (Sérsic index 0-2) and early-type galaxies (Sérsic index 2-8). The average radii of early-type galaxies are larger than late-type galaxies, as seen in Figure 4.12. As density increases in the population of late-type galaxies, radius increases, albeit a slight increase. The opposite is true for early-type galaxies, where galaxies in clusters are smaller in size than galaxies in the field. A more noticeable trend is that late-type galaxies are smaller in all environments than early-type galaxies, as can be seen by the average radius values. The histograms themselves show a steeper drop as radius increases in late-type galaxies than the drop in early-type galaxies. It should be noted that the early- and late-type galaxies are of different stellar masses in these bins based on Sérsic index. Based on Figure 4.5, as stellar mass increases Sérsic index also increases, leading to the conclusion that early-type galaxies are more massive than late-type galaxies. This is also consistent with our findings shown in Figure 4.9.

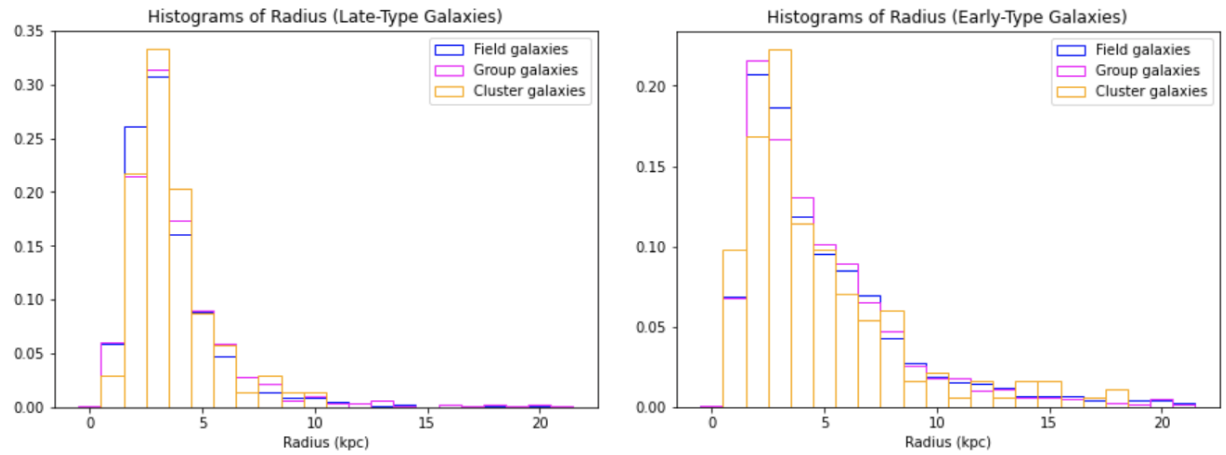


```
Average radius (kpc) (field) =  3.56
Average radius (kpc) (group) =  3.76
Average radius (kpc) (clust) =  3.78
```

```
Average radius (kpc) (field) =  5.17
Average radius (kpc) (group) =  5.16
Average radius (kpc) (clust) =  4.78
```

Figure 4.12. Normalized histograms of galactic radii in late-type (left) and early-type (right) galaxies with average radius in kpc printed for each environment.

4.5 Distance from Halo Center

The last property of galaxies observed in this study was the distance from a galaxy's dark matter halo center, for which plots in the three stellar mass bins are shown in Figure 4.13 (below). This factor may serve as a way to view transitional qualities of galaxies on a smaller scale than from field regions to clusters, as it gives insight to how galaxy morphology changes moving away from the densest part of a dark matter halo. These plots show an increasing Sérsic index for more massive galaxies, and as galaxies in field regions move further from their halo center, the galaxies become more disk-shaped.

For galaxies in clusters, the trend is less prominent, as is reflected in the printed averages below each plot. The Sérsic index of cluster galaxies remains fairly constant compared to the field and group galaxies in the different stellar mass bins.

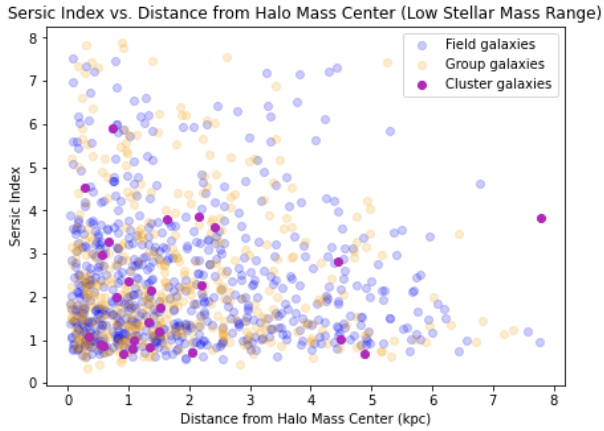

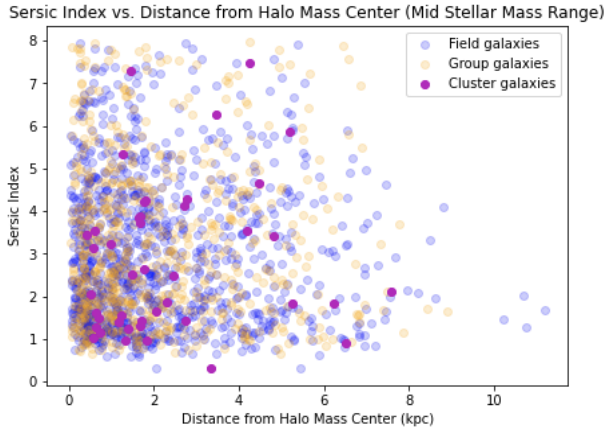


```
Average Sersic index (field) =  2.35
Average Sersic index (group) =  2.43
Average Sersic index (clust) =  2.16
```

```
Average Sersic index (field) =  3.01
Average Sersic index (group) =  3.18
Average Sersic index (clust) =  2.85
```

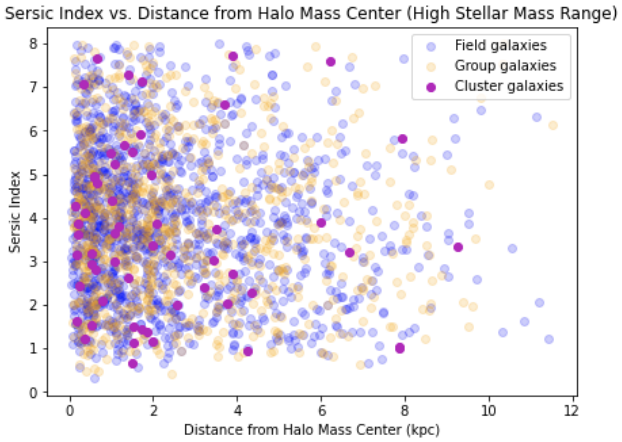


```
Average Sersic index (field) =  3.9
Average Sersic index (group) =  3.88
Average Sersic index (clust) =  3.65
```

Figure 4.13. Three plots of Sérsic index as a function of a galaxy's distance from its halo center in kiloparsec in the low stellar mass bin (top left), mid stellar mass bin (top right), and high stellar mass bin (bottom).

Chapter 5

Discussion

5.1 Consistency with Previous Findings

This section will be used primarily to compare the results of this study to those of previous studies. The main papers that will be referenced in this section are Weinmann et al. (2006), which addresses the dependence of color, specific star formation rate, and galactic morphology on halo mass. Similar studies that focus specifically on elliptical galaxies such as Naab et al. (2006) report similar findings to Weinmann et al. (2006). Ilbert et al. (2010) studied the effects of redshift on galaxy morphology, and discussed several possible mechanisms that link redshift, stellar mass, and other galactic properties. A study done by Vulcani et al. (2011) focuses on galaxy mass functions in clusters at low redshifts, and is referenced to compare results of changes in different stellar mass ranges. Lastly, Kuchner et al. (2017) and

Huertas-Company et al. (2013) focus on galactic size, and are mentioned in this section to compare observations of radius to.

Weinmann et al. (2006) discussed the trends seen in Sérsic index and SFR in different halo mass environments. To recap findings from this study, it was found that early-type galaxies appear more in high-density environments, take on elliptical shapes, and have low SFR, while late-type galaxies appear more in low-density environments, are disk-shaped, and have high SFR. In this particular study, Sérsic index was not used to classify galaxies as early- or late-type, however color and specific star formation rate (SSFR) were. Although Weinmann et al. (2006) did not quantify shape through Sérsic index, it was still observed that ellipticals appeared more in clusters while disks appeared more in field regions. Note that SSFR differs from SFR in that it reports SFR per unit mass, and can be calculated by dividing SFR by a galaxy's stellar mass. The Sérsic index and SFR data in this report show consistency with Weinmann et al. (2006), however these consistencies take place in different stellar mass bins. In the low stellar mass bin (log(10) - log(10.333)), SFR increases with density and Sérsic index increases with density; only the latter matches previous findings. This, on average, gives disk-shaped galaxies with low SFR. In the high stellar mass bin (log(10.666) - log(11)), SFR decreases with density and Sérsic index decreases with density; only the former matches previous findings. This gives elliptical galaxies with high SFR. While this defies previous findings, this discrepancy in Sérsic index and SFR in galaxies of different masses and in different environments may hint at one or more possible mechanisms at play that relate morphology to galactic environment. This will be further discussed in section 5.2.

In Figure 4.13, plots of Sérsic index as a function of the distance to the halo's center shows a stronger correlation in lower density regions than in clusters. As galaxies become more

massive, field and group galaxies tend to be more elliptical shaped, while this trend does not hold for cluster galaxies that remain elliptical at around Sérsic index of four. The distribution of field and group galaxies in all three stellar mass bins show a trend in which Sérsic index decreases with increasing distance from the halo center, which further solidifies the claims made by Weinmann et al. (2006) that disk galaxies appear more in less dense regions. Cluster galaxies in the lower stellar mass bins, however, are fairly evenly distributed despite distance from halo center.

Ilbert et al. (2010) observed that at low redshifts ($z < 0.8$), most massive quiescent galaxies were elliptical in shape. From the histograms shown in Figure 4.7 of Sérsic index in star-forming and quiescent galaxies, it can be concluded that the star-forming galaxies are generally more disk-shaped than quiescent galaxies, as is reflected in the average Sérsic indices for each environment. These results do not take stellar mass into account. Ilbert et al. (2010) concluded that based on the trends seen in massive quiescent galaxies and galactic shape, there must be a dominant mechanism that links SFR and a galaxy's structure that is present in at least high-mass galaxies.

Ilbert et al. (2010) also found 'blue ellipticals', where the blue color in galaxies tends to signify high SFR; however, the fraction of blue ellipticals was found to decrease as stellar mass increased. This is inconsistent with our findings in the high stellar mass bin of Figure 4.6, which indicates a larger amount of star-forming ellipticals than in the lower and mid stellar mass bins. Figure 5.1 (below) shows a plot of the percentage of blue ellipticals as a function of logarithmic stellar mass taken from the Ilbert et al. (2010) report. It is clear that at all redshifts, the fraction of blue elliptical galaxies decreases as stellar mass increases, but as redshift increases the fraction of blue ellipticals drops more steeply. It is important to note that the galaxies cataloged

by Yang et al. (2005) are of lower redshift than is reported by Ilbert et al. (2010) at $0.01 < z < 0.20$. Because of the apparent correlation between redshift, stellar mass and the fraction of blue ellipticals, it is likely that the fraction of blue ellipticals decreases at a slower rate for the galaxies used in this study. To confirm whether or not this is true, another study following methods used by Ilbert et al. (2010) at lower redshifts should be conducted.

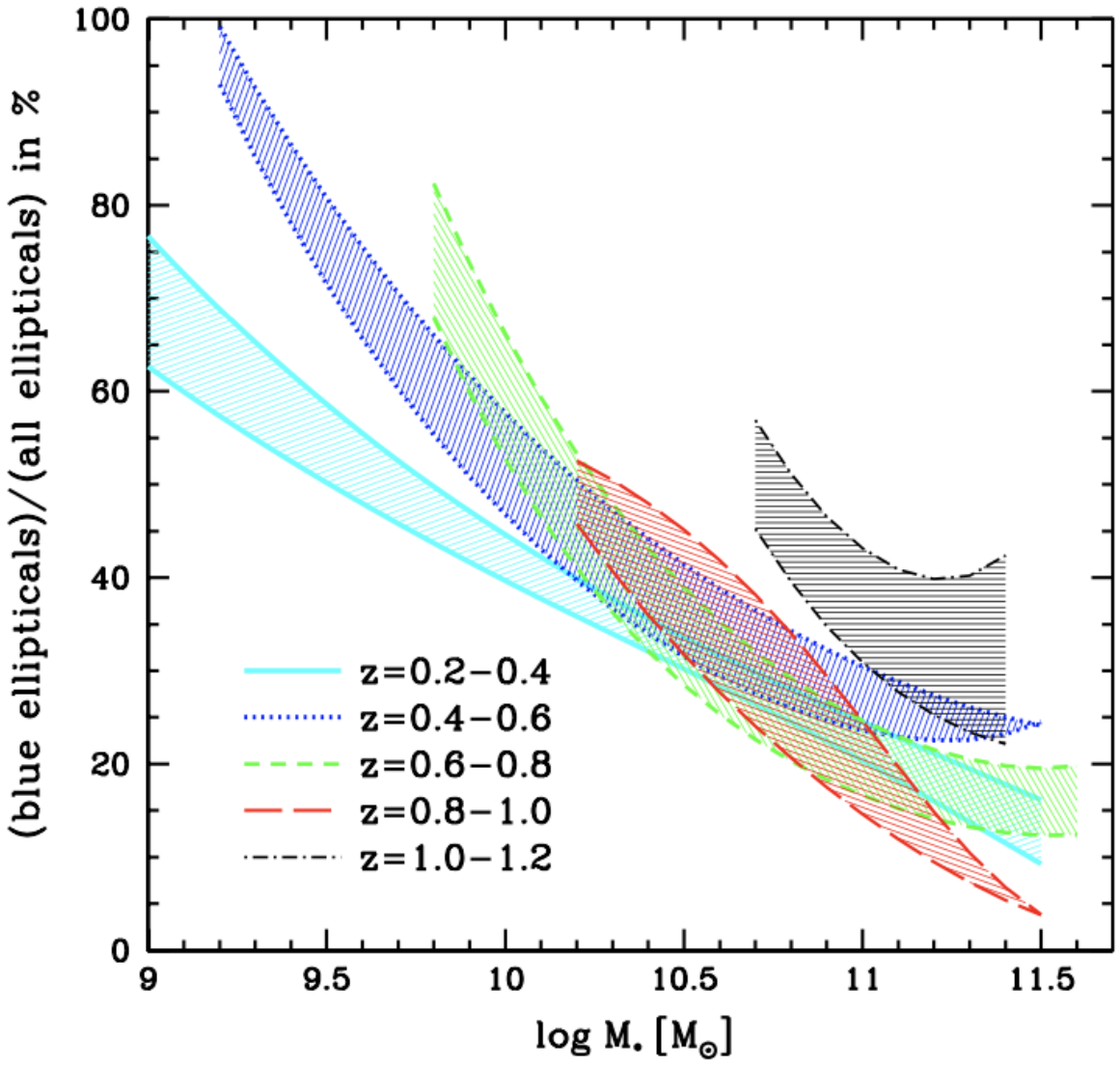

Figure 5.1. (Figure 22 in Ilbert et al. (2010)). This plot shows the percentage of star-forming elliptical galaxies plotted against the logarithmic stellar mass in units of solar mass. Our findings report galaxies of stellar mass log(10) to log(11) at redshifts of 0.2 to 0.4.

It has been suggested in previous studies that less massive galaxies (stellar mass below 10^{11}solar mass) display significant evolution compared to higher mass galaxies (stellar mass above 10^{11}solar mass) at redshift less than 1 (Vulcani, Poggianti, Aragón-Salamanca et al. 2011).

This is confirmed in Figure 4.6 that shows Sérsic index changing in the three stellar mass bins; low-mass galaxies peak at 1 before dropping steeply, whereas high-mass galaxies peak at Sérsic index 2 and 4 in different environments, nonetheless undergoing less of a steep drop compared to low-mass galaxies. However, this claim is contradicted by Figure 4.3, where SFR displays a more significant change in the high stellar mass galaxies. The peak in SFR is seen to reach about 2.5 and drop immediately to less than 0.5 in the high stellar mass bin. Vulcani et al. (2011) mentions the possibility of a quasi-universal mass function for each classification of galaxy as previous studies did not find correlation between stellar mass and environment. However, these previous studies mostly focus on galaxies in field regions.

Previous studies found that early-type galaxies are smaller in size than late-type galaxies (Kuchner, Ziegler, Verdugo et al. 2017). However, viewing radius in histograms in the two Sérsic index bins (late-type and early-type) in Figure 4.12, one can see that the size of early-type galaxies is larger than that of late-type galaxies. This is inconsistent with Kuchner et al. (2017). Figure 4.11, however, which shows histograms of radius in bins of star-forming vs. quiescent galaxies, shows that star-forming galaxies are larger than quiescent galaxies. Using SFR to classify galaxies as early- or late-type then proves consistent with previous studies. A discrepancy between galactic radius and SFR may be the cause of this as is mentioned by Kuchner et al. (2017). From the plots and histograms of galactic radius with bins of stellar mass, it appears that environment has no noticeable effect on galaxy size. This is consistent with findings from the previously mentioned study by Huertas-Company et al. (2013).

5.2 Possible Mechanisms at Play

Based on the three histograms in different stellar mass ranges of Sérsic index shown in Figure 4.6, it is clear that more massive galaxies take on a more elliptical shape, while less massive galaxies are generally more disk shaped in the field region. There are three proposed explanations for this observation. The first is that in the case of a merger event between two late-type galaxies, the stellar orbits within the galaxies may be randomized so that they no longer fall in line with the original disk-shape. This would in turn cause the galaxy to appear more elliptical in shape with a higher Sérsic index. This scenario would explain the high population of early-type galaxies in the field region as seen by the Sérsic index vs. stellar mass plot in Figure 4.5.

The second possible explanation for the trend in Sérsic index in different environments is that in galaxy-galaxy mergers, gases move to the center of the galaxies and increase star formation rate towards the center. This aligns with both the Sérsic index and SFR histograms, as SFR unexpectedly increases as density increases in the lower stellar mass range as seen in Figure 4.3. This would also make sense to explain the trend that can be seen at lower masses where disks are clearly converting to elliptical galaxies, which is reflected in the fact that the average Sérsic index changes more steeply from field to cluster than in the other stellar mass bins. The third explanation would be a combination of the previous two mechanisms, as both relate to galaxy mergers. It is previously argued that galaxy mergers result in size growth; however, there are many conflicting findings in previous studies when it comes to low-redshift galaxies. According to Huertas-Company et al. (2013), there is little evidence of environmental

dependence on the size low-redshift galaxies, which is what aligns with the results found in this study as seen in Figure 4.10.

When viewing the SFR plots, it is clear from Figure 4.3 that more massive galaxies have overall lower SFR. This may be due to the fact that galaxies with higher stellar mass have existed in their environments for an extended period of time compared to lower stellar mass galaxies, which may point to a possibility of strangulation stripping as this mechanism exhibits a long time scale. In Figure 4.4 that shows SFR histograms indexed by bins of early- and late-type galaxies, it is confirmed that late-type galaxies have an overall higher SFR than early-type galaxies. This again may be due to the merger events that take place in the different environments.

The discrepancies seen between Sérsic index and SFR in this study's different stellar mass ranges from previous studies' findings may point at inconsistency in using Sérsic index and SFR to define early- and late-type galaxies. In the case of ram pressure stripping and strangulation, a galaxy's Sérsic index would remain the same regardless of SFR. This may also serve as an explanation for the discrepancies in SFR and Sérsic index readings in the different stellar mass bins, observed in Figures 4.3 and 4.6. However, based on the 2015 study conducted by Peng, Miaolino & Cochrane, strangulation would likely lead to an increase in stellar mass. In this case, there should be a higher number of high-mass galaxies with low SFR, which is in fact observed in Figures 4.2 and 4.3. In Figure 4.2, there is clearly a higher number of quiescent galaxies near the higher end of the stellar mass axis, and in Figure 4.3, more of the galaxies in the histogram indexed as the high stellar mass bin have low SFR. This would, as a result, point to strangulation as a mechanism at play as opposed to ram pressure stripping.

Another possibility is that SFR is more affected than structure in low mass galaxies (Kuchner, Ziegler, Verdugo et al. 2017). However, because the SFR histograms seen in Figure 4.6 are inconsistent in the low stellar mass range, this may disagree with the claim made by Kuchner et al. (2017). Another explanation to the changes in SFR where Sérsic index is not affected is feedback from Active Galactic Nuclei on the satellite galaxies of a massive halo (Ilbert, Salvato, Le Floc'h et al. 2010; Cattaneo, Dekel, Devriendt, et al. 2006). However, the N-body simulations by Cattaneo et al. (2006) to conclude this fact focused more on $z \sim 1$ and above redshifts.

Kuchner et al. (2017) further investigated the stellar-mass–size relationship in galaxies. Based on the trends seen in Figure 4.11 of galactic radius in star-forming and quiescent galaxies, star-forming galaxies are larger than quiescent galaxies in lower density environments. When using SFR to determine a galaxy's classification as early- or late-type, this result is consistent with previous findings unlike when Sérsic index was used. Possible explanations for this trend is that gas is less strongly bound to the outermost parts of a disk galaxy as is determined by gravitational potential energy, and so will be removed first. This will not only cause a decrease in galactic radius, but will also strip the galaxy's outskirts of the gas necessary to form stars, leading to a drop in SFR as well. However, this scenario should lead to a trend in radius and stellar mass as both relate to gravitational potential energy, but this trend is not observed in Figure 4.10. Tidal stripping may further contribute to the loss of the disk's outermost gas (Kuchner, Ziegler, Verdugo et al. 2017).

Chapter 6

Conclusions

This study aimed to determine the effect environment has on galaxy morphology, as well as other properties of galaxies such as SFR. By using data from the Yang et al. (2005) group catalog in SDSS Data Release 7 and the high viewing capabilities of the HSC-SSP, several conclusions can be drawn about galaxies at low-redshift in different environments, defined as the field region, groups of galaxies, and galaxy clusters. Section 5.3.1 will discuss trends observed in galaxy morphology relating to Sérsic index, SFR, stellar mass, and radius. Section 5.3.2 will generalize the possible physical mechanisms that lead to the observations.

6.1 Trends in Galactic Morphology

The following conclusions about trends in galaxy morphology and behavior can be drawn from the data presented in this study:

(1) Sérsic index, SFR and stellar mass are all properties of a galaxy that change with environmental density based on dark matter halo mass.

(2) Star-forming galaxies are on average more disk-shaped than quiescent galaxies in the field and group environments; however, in clusters, there is less of a correlation as seen in Figure 4.8.

(3) A galaxy's size exhibits little to no environmental dependence with stellar mass, but does align with bins of Sérsic index to show that late-type galaxies are generally smaller than early-type galaxies. Conversely, the data shows that star-forming galaxies are larger than quiescent galaxies in the field and group, environments, but quiescent galaxies are larger in clusters.

The inconsistency in using Sérsic index and SFR as means to classify galaxies as early- and late-type is brought to light by this third conclusion. It is likely the case that the environmental dependence for these instances is characterized by one or more mechanisms that affect SFR without affecting the galaxy's shape.

6.2 Theorized Mechanisms

This section will focus on the conclusions drawn regarding the possible physical mechanisms that affect the galaxies in this study, and may serve as explanations for the trends seen in section 5.3.1.

(1) Galaxy mergers likely play a large role in explaining the trends in galaxy morphology seen in this data and many previous studies. Mergers may lead to an increased SFR, as well as an increased Sérsic index, which is seen in the lower stellar mass bins of each properties histograms (Figures 4.3 and 4.6). Proof of galaxy mergers include:

   (a) The high population of high-mass elliptical galaxies in the field region compared to that of high-mass disk galaxies

   (b) The high population of early-type galaxies in the field regions

(2) Strangulation is favored over ram pressure stripping to explain the discrepancies in Sérsic index and SFR in the different mass ranges because many high-mass galaxies exhibit low SFR. This aligns with previous studies done that claim that the theorized timescale of strangulation is favored over that of ram pressure stripping.

There are likely several contributing factors that lead to galaxy evolution that both encourage and counteract the effects of galaxy mergers and ram pressure stripping. Examples mentioned in this report are feedback from AGN and tidal stripping that cause a drop in SFR. Because there are so many different ways to define a galaxy's classification– i.e. through Sérsic index, SFR, and color– and so many factors that lead to galaxy evolution, finding trends and discussing possible mechanisms that lead to the trends is a challenge. By looking at a more narrow focus, extragalactic astronomers may be better able to pinpoint the causes of the observed bimodality in galaxies. For example, looking at trends in SFR, Sérsic index, and size in galaxies of similar mass at low-redshifts would decomplicate the trends by diminishing effects of stellar mass. Because this data appears to favor strangulation over ram pressure stripping, it may be worthwhile to also look at color and stellar metallicity of galaxies to confirm this fact.

While the results of this study present a new perspective on galaxy morphology and its dependence on environment, much more work needs to be done to fully understand galaxy evolution. In addition to future studies holding certain galaxy characteristics fixed, more studies should look to employ powerful survey instruments similar to the HSC-SSP in order to expand and improve datasets.

Acknowledgments

I would like to extend a huge thank you to my research advisor, Dr. John Silverman at the University of Tokyo and Kavli Institute of Physics and Mathematics of the Universe in Japan. Without his willingness to take on an undergraduate researcher from across the world, let alone during the COVID-19 pandemic, I would not have had the opportunity to conduct extragalactic research. After several late-night and early-morning meetings, I am thankful for all of the time he dedicated to helping me improve my research techniques and answer my questions. Dr. Silverman also introduced me to Xuheng Ding, a graduate student at UCLA, whom I would like to thank for the many hours spent explaining the different aspects of his Decomprofile code to me, as well as helped me understand new computational methods this year.

I was introduced to Dr. Silverman my junior year by Dr. Mauro Giavalisco, who is my academic advisor at UMass Amherst. I told Dr. Giavalisco as a sophomore that I wanted to conduct research abroad, with which he responded with great enthusiasm and support. After several months of planning, my trip to Japan was nearly booked before the pandemic hit. Regardless of my in-person or virtual research experience, Dr. Giavalisco has encouraged me to continue working hard throughout my undergraduate career.

I would also like to thank Dr. Min Yun, who is the UMass Astronomy Department Honors Program Director. His involvement in my research opportunity and the writing of this thesis is greatly appreciated. Dr. Yun was kind enough to introduce me to now-UMass alumnus Kenneth Lin, who provided me with ample advice on traveling and astronomical research.

Last, I would like to express my gratitude for the UMass Astronomy Department as a whole for the amazing opportunities I have been given as an undergraduate student. Without the connections of the university and without the kindness and enthusiasm of the faculty, I would not have been given this amazing international research opportunity.

References

Aihara H, AlSayyad Y, Ando M, Armstrong R, Bosch J, et al. 2019. *Publications of the Astronomical Society of Japan*. 71(6):114

Birrer S, Amara A. 2018. *Physics of the Dark Universe*. 22:189–201

Blanton, Michael R., Schlegel, David J., Strauss, Michael A. 2005. *AJ*. 129(6):2562–78

Blanton MR, Hogg DW, Brinkmann J, Connolly AJ, Csabai I, et al. 2003. *ApJ*. 592(2):819–38

Bowen IS, Vaughan AH. 1973. *Appl. Opt., AO*. 12(7):1430–35

Burg RFJ van der, Hoekstra H, Muzzin A, Sifón C, Viola M, et al. 2017. *A&A*. 607:A79

Cattaneo A, Dekel A, Devriendt J, Guiderdoni B, Blaizot J. 2006. *Monthly Notices of the Royal Astronomical Society*. 370(4):1651–65

Contopoulos, George, Efthymiopoulos, Christos. 2011. *Scholarpedia*

Dressler A. 1980. *The Astrophysical Journal*. 236:351–65

Greco JP, Greene JE, Strauss MA, Macarthur LA, Flowers X, et al. 2018a. *ApJ*. 857(2):104

Greco JP, Greene JE, Strauss MA, Macarthur LA, Flowers X, et al. 2018b. *ApJ*. 857(2):104

Grützbauch R, Conselice CJ, Varela J, Bundy K, Cooper MC, et al. 2011. *Mon Not R Astron Soc*. 411(2):929–46

Gunn JE, Gott JR III. 1972. *ApJ*. 176:1

Gunn JE, Siegmund WA, al EJM et. 2006. *AJ*. 131(4):2332–59

Holtzman JA, Harrison TE, Coughlin JL. 2010. *The NMSU 1 m Telescope at Apache Point Observatory*. Advances in Astronomy. https://www.hindawi.com/journals/aa/2010/193086/

Huertas-Company M, Shankar F, Mei S, Bernardi M, Aguerri JAL, et al. 2013. *ApJ*. 779(1):29

Ilbert O, Salvato M, Le Floc'h E, Aussel H, Capak P, et al. 2010. *ApJ*. 709(2):644–63

Karouzos M. 2019. *Nat Astron*. 3(2):139–139

Kauffmann G, Li C, Zhang W, Weinmann S. 2013. *Monthly Notices of the Royal Astronomical Society*. 430(2):1447–56

Kauffmann, Guinevere

Kawata, Daisuke, Mulchaey, John S. 2008. *The Astrophysical Journal Letters*. 672(2):L103

Kodama T, Smail I, Nakata F, Okamura S, Bower RG. 2001. . 562(1):5

Kuchner U, Ziegler B, Verdugo M, Bamford S, Häußler B. 2017. *A&A*. 604:A54

Miyazaki S, Iwata I. , p. 30

Moore, Ben, Katz, Neal, Lake, George. 1996. *Nature*. 379(6566):613–16

Naab T, Khochfar S, Burkert A. 2005. *arXiv:astro-ph/0509667*

Pannella, Maurilio, Gabasch, Armin, Goranova, Yuliana, Drory, Niv, Hopp, Ulrich. 2009. *The Astrophysical Journal*, pp. 787–803

(PDF) Loose Groups of Galaxies in the Las Campanas Redshift Survey. https://www.researchgate.net/publication/231034123_Loose_Groups_of_Galaxies_in_the_Las_Campanas_Redshift_Survey

(PDF) Loose Groups of Galaxies in the Las Campanas Redshift Survey. https://www.researchgate.net/publication/231034123_Loose_Groups_of_Galaxies_in_the_Las_Campanas_Redshift_Survey

Pearson WJ, Wang L, Alpaslan M, Baldry I, Bilicki M, et al. 2019. *A&A*. 631:A51

Peng Y, Maiolino R, Cochrane R. 2015. *Nature*. 521(7551):192–95

Petrosian V. 1976. *ApJ*. 210:L53

Postman M, Geller MJ. 1984. *ApJ*. 281:95

Rachel Mandelbaum. *Galaxy halo masses and satellite fractions from galaxy–galaxy lensing in the Sloan Digital Sky Survey: stellar mass, luminosity, morphology and environment dependencies | Monthly Notices of the Royal Astronomical Society | Oxford Academic*. https://academic.oup.com/mnras/article/368/2/715/984946

Schawinski, Kevin, Dowlin, Nathan, Thomas, Daniel, Urry, C. Megan. 2010. *The Astrophysical Journal Letters*

Sparke LS, Gallagher JS. 2007. *Galaxies in the universe: an introduction*. Cambridge ; New York: Cambridge University Press. 431 pp. 2nd ed ed.

Tanaka M, Goto T, Okamura S, Shimasaku K, Brinkmann J. 2004. *AJ*. 128(6):2677–95

Tempel E, Saar E, Liivamägi LJ, Tamm A, Einasto J, et al. 2011. *A&A*. 529:A53

Umetsu K, Sereno M, Lieu M, Miyatake H, Medezinski E, et al. 2020. *ApJ*. 890(2):148

Vulcani B, Poggianti BM, Aragón-Salamanca A, Fasano G, Rudnick G, et al. 2011. *Monthly Notices of the Royal Astronomical Society*. 412(1):246–68

Weinmann SM, Bosch FC van den, Yang X, Mo HJ. 2006. *Monthly Notices of the Royal Astronomical Society*. 366(1):2–28

Yang X, Mo HJ, Bosch FC van den. 2008. *ApJ*. 676(1):248–61

Yang X, Mo HJ, van den Bosch FC, Pasquali A, Li C, Barden M. 2007. *ApJ*. 671(1):153–70

Zabludoff AI, Mulchaey JS. 1998. *ApJ*. 496(1):39–72